Polynomial System Identification Modeling and Adaptive Model Predictive Control of Arterial Oxygen Saturation in Premature Infants

---

A Thesis presented to the Faculty of the Graduate School University of Missouri – Columbia

---

In Partial Fulfillment

Of the Requirement of the Degree

Master of Science

By

RICHARD H. DUTTON

Dr. Roger Fales, Advisor

December 2020

The undersigned, appointed by the Associate Vice Chancellor of the Office of Research and Graduate Studies, have examined the thesis entitled

POLYNOMIAL SYSTEM IDENTIFICATION MODELING AND ADAPTIVE MODEL PREDICTIVE CONTROL OF ARTERIAL OXYGEN SATURATION IN PREMATURE INFANTS

Presented by Richard H. Dutton,

a candidate for the degree of Master of Science

and hereby certify that, in their opinion, it is worthy of acceptance.

_____

Professor Roger Fales

_____

Professor Craig Kluever

_____

Professor Steve Borgelt

Acknowledgements

First and foremost, I want to thank Dr. Roger Fales for his technical guidance, expertise, and especially, his patience on this research endeavor. His cheery demeaner, and truly approachable personality, made all the years of hardship worth it. I will forever be grateful to have had you are my graduate advisor; as I want to believe I grew as an engineer under your tutelage for assisting me in solving a problem that had literally millions of possible solutions.

In addition, I would like to thank both Dr. Craig Kluever and Dr. Steve Borgelt for taking the time to serve as members of my thesis committee. If it were not for Dr. Kluever's Dynamic Systems and Controls course; I doubt I would have fallen in love with control theory. I also had the pleasure of taking Dr. Steve Borgelt's Professional Development in Engineering. Such a course showed how to ethically carry one's self in the engineering profession.

I would also like to thank my those who kept giving me encouragement finish this project. Tyler Shinn, for being the calm in the storm that was graduate school. Zachary Wagner, for believing in me as we worked together in the graduate offices, making the stress of graduate research feel special. Dr. Juan Cockburn, Matthew Brown, Everett Kleven, Edward Pewitt, Trina Le, Dr. Sankalp Bhan, and Jon Marble; for always encouraging me to keep going in the face of doubt. Finally, I want to thank my family. They kept me going and cheerful in private from the creep of uncertainty.

Table of Contents

Table of Figures

Table of Tables

Abstract

The automation of the regulation of the fraction of inspired oxygen (FiO_2) in neonatal mechanical ventilation to treat respiratory distress syndrome has proven challenging due to competing objectives: maintaining arterial oxygen saturation levels (SpO_2) while simultaneously not inducing complications such as retrolental fibroplasia. Historically, models of the dynamics of the neonatal respiratory system were first order transfer function approximations. This work used higher order polynomial system identification methods with the model structures of autoregressive with exogenous inputs (ARX) and Box-Jenkins (BJ) models to investigate possible improved modeling of the dynamic relationship between the FiO_2, Heart Rate (HR), and Respiratory Rate (RR) to the SpO_2. Through a parameter sweep of different of polynomial orders and sampling delays, 3,456 ARX models and 13,176 BJ models were created, with four being selected for comparison based upon modeling performance metrics. From these best performing models, it was concluded that the FiO_2 relationship to SpO_2 could still be adequately approximated by a first order transfer function model with delay. The disturbance HR, RR, and the unmodeled dynamics did require higher order approximations. It was also shown that selecting a model based off the Akaike's Information Criterion was preferred in picking a model from a collection of identified models.

With a singular winning model from the four best performing models, an adaptive model predictive controller (AMPC) was designed to adhere to clinical best practices to regulate the SpO_2. Through a recursive polynomial model estimator (RPME), an ARX approximation of the unknown model's dynamics for the FiO_2, HR, and RR relationship to the SpO_2 could be used to update the internal model of the AMPC. Through this online

model estimation, the AMPC could successfully feedforward reject the HR and RR disturbances improving the simulated time within the SpO_2 target limits, 67.8% of simulation time, to a baseline PI controller's 56.6%, in periodic desaturation simulations.

1 Introduction

1.1 Background

One of the most frequent systematic diseases in the neonatal intensive care unit (NICU) is respiratory distress syndrome (RDS), formally known as *hyaline membrane disease*. Such a disease affects 60% of infants below 28 weeks of gestation and 30% of infants born between 28 and 34 weeks of gestation. This is primarily caused by the underdevelopment of the lungs and the resulting lack of surfactants. These surfactants reduce the surface tension of the alveoli which then reduces the pressures needed to keep the lungs inflated [1].

The standard treatment for RDS begins with vigorous respiratory support through regulation of warm, humidified, oxygen enriched gases through the level of fraction of inspired oxygen (FiO_2) into the lungs [2]. While for milder RDS an oxygen hood alone might be sufficient to maintain adequate oxygen tissue levels, more serious or more frequent RDS cases would require mechanical ventilation. The most common mechanical ventilation methodology is continuous positive-airway pressure (CPAP), which is administered through either nasal prongs or endotracheal intubation [3].

The goal of these devices is to maintain the true measurement of the body's oxygen saturation levels, known as the partial pressure of oxygen in the arterial blood (PaO_2), which is typically given in mmHg. Yet, measuring PaO_2 is inconvenient and difficult, having to be measured through a probe in the clamped umbilical cord [4]. A more convenient and readily available proxy for PaO_2, is the arterial oxygen saturation (SaO_2), a common and easily obtained medical signal [5]–[8]. The SaO_2 of a neonate is typically

monitored using a pulse oximeter. The measurement of a SaO_2 from pulse oximetry is referred to as a SpO_2 value. Both SaO_2 and SpO_2 are percentage measurements. Pulse oximeters measure arterial hemoglobin through the tissue absorption of two distinct wavelengths of light, 660mm and 940mm. Accuracy of pulse oximeters have been claimed to ±2% when the overall SpO_2 saturation is above 70% [9]. Research into the effectiveness of the pulse oximeters for reading SpO_2 have shown reliable oxygenation measurements in infants with chronic lung disease, but ability to detect hyperoxia has remained controversial [7].

While oxygen is one of the most commonly used therapeutic agents [10], it can still carry with it significant complications if overused, especially in the NICU population. A common neonatal complication due to tissue hyperoxia, too much tissue oxygen, is retrolental fibroplasia. Retrolental fibroplasia, more commonly known as retinopathy of prematurity (ROP), is the inhibition of the growth of the vascular retinal vessels when under high levels of supplemental oxygen. Such excessive vascular proliferation could eventually lead to complete retinal detachment [5]. Additionally, there is evidence that the still developing neonatal physiology is susceptible to brain damage from hyperoxia due to underdeveloped self-regulation [6]. As a result, the regulation of supplemental oxygen in the neonatal patient is a constantly competing objective between the immediate neonate survival from tissue hypoxia and the long term hyperoxia complications.

Currently, the majority of NICU regulation and monitoring of SpO_2 is performed using manual adjustments from alarms for both desaturation events and hyperoxia. A desaturation event is defined as the SpO_2 going below the target values for a prolonged period. This manual control has often been seen as in need of improved efficacy with

neonates under supplemental oxygen only staying within the target ranges as little as 31% of the time [11]. Even then, the target ranges themselves are debated [5], [7], [11], [12].

1.2 Literature Review

1.2.1 Prior modeling work

The first mathematical modeling of the human respiratory system came from Gray [13]. The research performed by Gary only looked at steady state response, with delays and nonlinear dynamics not added until Grodins [14]. Grodins focused mostly on the chemical modeling of the respiratory system under either acidosis or alkalosis. The first attempt at modeling the dynamics of humans under mechanical ventilation came from Grevisse, which focused on modeling through physically available variables [15]. Grevisse split the modeling of the human respiratory system into a three-sub model system: an ideal gas exchange compartment, a dead space compartment, and a blood flow shunting compartment.

More modern modeling methods begin in with Yu [16]. Yu modeled the FiO_2 to PaO_2 dynamics with a first order transfer function approximation. This first order transfer function was then extended to SaO_2 through a linearization of the PaO_2 to SaO_2 curve. Fathabadi investigated the validity of the first order transfer function model between the FiO_2 and SpO_2 and found that only 37% could be characterized as a first order response [17]. Fathabadi expanded on this later when investigating the characteristics of first order response and concluded that the first order transfer function model could not be represented by positive FiO_2 adjustments alone [18].

1.2.2 Prior automated supplemental oxygen control work

The first published work of the closed loop control of premature infants came from Beddis [19]. In that work, the feedback variable was the PaO_2 and the FiO_2 adjustments were restricted to be explicitly 5% when sampled at a 1-minute interval. In this first attempt at the automated regulation of supplemental oxygen in premature infants, the automated control was able to maintain within the target range 27.6% of the time compared to the manual control target range satisfaction of just 12.2%. None the less, the servo controller increased the amount of time above the target limits compared to the manual control. The work of Beddis also began the standard of neonatal mechanical ventilation regulation controller performance benchmarking by percent of time within target limits.

The other major published controller design for the regulation of the supplementary oxygen for neonates where PaO_2 was the regulated variable came from Dugdale [20]. In that study, the controller picked was both static and tuned on singular step inputs of premature infants with "…safety and conservatism very much in mind." At the time, it was felt that adaptive control literature had not matured enough for its use in such a critical environment as the NICU.

Yu [16] used a multiple-model adaptive controller (MMAC) that regulated SaO_2 through a weighted collection of proportional-integral (PI) controllers. Each PI controllers was tuned on six linear first order approximations of the PaO_2 response to FiO_2 adjustments with a nonlinear gain from the PaO_2 to SaO_2 curve. The MMAC would then adaptively combine the weights of the different controllers to produce a final FiO_2

action. The MMAC was shown to successfully regulate SaO_2 in both simulation and animal studies.

Urschitz and Seyfang [21] created an artificial intelligence based temporal abstraction controller whose goal was to create as few adjustments as possible. This is accomplished by operating through a series of modes with two main "spreads", the state spread, and the trend spread. The state spread focused on the state of the system over a five-minute window to classify the data into either too high, too low, or somewhere in between. The trend spread does the same, but on a much smaller one-minute window. In a clinical trial, this algorithm was shown to improve compliance to the SpO_2 target range over the manual control [22].

Morozoff [23] clinically tested three controller designs on seven neonatal patients: a state machine, an adaptive model controller, and a PID controller. The state machine looked at the SpO_2 error, error velocity, and error acceleration to build a system of rules. The PID was designed to be tuned by the end user, while the adaptive model controller used a table lookup of the oxygen dissociation curve between PaO_2 and the SpO_2. All these controllers were baselined to the normal manual control from the staff. The two conclusions from the paper was that all three controllers performed better than the manual control and that the adaptive controller was the preferred choice. The adaptive controller was preferred as it was able to slightly perform better than the other controllers while requiring significantly less tuning.

Claure [24] performed a large multicenter study with thirty two infants at four different hospitals. The controller that was used was not explicitly described but believed to be a stepwise basal FiO_2 controller where the FiO_2 is analyzed every second and

adjusted depending upon whether the SpO_2 was meeting the required ranges. It was shown none the less that the automation of the FiO_2 regulation decreased not only the amount of time within the prescribed ranges by 8%, but also significantly reduced the overall workload on the NICU staff.

1.2.3 Prior work at the University of Missouri

The University of Missouri-Columbia (UMC) has been investigating the automation of the SpO_2 levels in premature infants through FiO_2 control since their first published works in [25]–[27]. In addition to these published works, four graduate students presented their thesis and dissertations for the goal of modeling and controlling the FiO_2 in the NICU [28]–[31]. Additionally, an unpublished work by another graduate student includes a systematic method of finding FiO_2 modeling events [32].

The UMC modeling and control work began with the collection of manual control data by Keim [28] at the Columbia Regional Hospital, now known as the Women's and Children's Hospital. The measurements collected were FiO_2, heart rate (HR), respiratory rate (RR), and SpO_2. A further description of the data collection used by [28] is given in section 2.1. Keim also developed a time varying nonlinear model expanding upon the FiO_2 to SaO_2 relationship from [16] with the SaO_2 to SpO_2 curves from [33] . This nonlinear model was then compared to the clinical data for verification [25], [28].

For real time estimating of the recovery relationship between the collected FiO_2 and SpO_2 measurements, three different techniques were investigated: a dynamic fuzzy logic system (DFLS), an continuous time parameter-estimating extended Kalman filter (CPE-EKF), and a discrete time parameter-estimating extended Kalman filter (DPE-

EKF). It was concluded that the DPE-EKF could most accurately estimate the unknown parameters as well as translate best to linear control theory [27].

From these investigations, three control designs were then developed and evaluated on their ability to maintain SpO_2 levels in the face of unknown disturbances. These three controllers included a μ-synthesis robust controller, a static PI controller, and an adaptive controller using the DPE-EKF to determine the FiO_2 to SpO_2 gain. The adaptive DPE-EKF performed the best and was developed into UMC's first prototype automatic FiO_2 controller [28].

Krone analyzed the data collected by [28] to try and model not only the FiO_2 to SpO_2 relationship, but possibility of being able to model the relationship between the HR and RR to the SpO_2 as possible measured disturbances. While a conclusion was made that there was a distinct and quantifiable first order relationship between the FiO_2 and the SpO_2, no quantitative relationship was possible for the HR and RR. The relationship between HR and RR to the SpO_2 dynamics was left to visual inspection alone [29].

To attempt to model the relationship between these three inputs and the SpO_2, Krone developed a fuzzy logic, neural network, and dynamic transfer function model. These models were simulated and compared the best model being able to predict SpO_2 clinical measurements the longest. At the conclusion of the simulations, it was determined that the dynamic transfer function model was the strongest modeling choice [26], [29]. The dynamic transfer function model though would often predict significantly smaller gains for the HR and RR than the FiO_2, with the HR and RR possibly even having negative dc gains.

From this dynamic transfer function model, three different control designs were once again developed. The first controller design was a linear quadratic regulator proportional integral controller (LQR-PI) where the FiO_2 to SpO_2 dynamics were regulated with the HR and RR considered disturbances. The second controller was an H_∞ using six different μ-synthesis ranges of possible FiO_2 gains and time constants, and the third controller was an adaptive controller with feedforward disturbance rejection based off of the derivative of the HR and RR. While it was shown that all three controllers could reject the disturbances from the HR and RR and maintain the SpO_2 with the target range, it concluded that the H_∞ controller was the best performing controller, even though it was the most aggressive with FiO_2 adjustments.

Quigley [30] developed a series of six robust controllers, using the best practices outlined by Chow [5], on the dynamic transfer function model found by [29]. Using a genetic algorithm (GA) to pick the both the most appropriate nominal plant, and offline prepared robust controller. The HR and RR inputs from the dynamic transfer function model were left for the purposes of simulation. These inputs were not used for feedforward disturbance rejection as the GA was only estimating parameters, and thus nominal models and robust controllers from just the FiO_2 to SpO_2 relationship.

Faqeeh's [31] primary investigation was on the use of an adaptive proportional-integral (PI) controller in both a hardware-in-the-loop (HIL) and clinical testing. These adaptive PI controllers would assume a FiO_2 and SpO_2 first order transfer function plant model with no delay. The adaptation nature of these controllers came using a Parameter Estimating Extended Kalman Filter (PE-EKF) to estimate the first order gain and time constant of the unknown models. For the HIL testing of the adaptive PI controller, a

sweep was performed through all of the combinations of the three most common gain and time constant presented in [29]. The goal of the HIL testing was to see if not only the SpO_2 could be satisfactorily regulated, but that the first order parameters were being adequately estimated by the PE-EKF. Additionally, this system was tested in a clinical environment on two human subjects and showed its feasibility to minimize the variability of the SpO_2.

Shinn [32] showed the ability to estimate the first order parameters of the neonatal SpO_2 response to FiO_2 adjustments through the use of an extended Kalman filter. To preprocess the data, the forward difference derivative of the FiO_2 signal was calculated to automate the identification of FiO_2 adjustment events for modeling. A limitation of the work was that it was limited to positive FiO_2 adjustments with no attempt to explicitly model the delay between the FiO_2 and SpO_2 response. This limitation was shown by [18] to be a significant omission in the modeling of the dynamics of the neonate.

1.3 Research Objectives

In this research, a systematic approach was developed to investigate the viability of finding a singular, higher order model to go beyond the lower order FiO_2 to SpO_2 first order transfer functions that have been previously investigated in the literature. To find data for modeling, an automated process for finding recovery events with both positive and negative FiO_2 adjustment must be established. An additional objective within this research was to not add additional prefiltering of the data used for model estimation. Furthermore, was the desire to expand upon the HR and RR to SpO_2 transfer function models from [29] with both explicit delay and higher order model estimations.

From these higher order models, the adaptive feedforward controller developed by [29] could be further advanced through a change to an adaptive model predictive controller (AMPC) architecture. Through this architecture, the measured disturbances of HR and RR could be feedforward rejected. Moreover, the AMPC can incorporate the best practices more easily outlined by [5]. While the concept of model predictive control has been applied to neonatal incubators [34], model predictive control to the regulation neonatal SpO_2 is novel.

Thusly, the following is a summary of the objectives of this research:

- The automation of FiO_2 recovery event finding with both positive and negative adjustments during recovery.
- The use of classical system identification techniques to investigate higher order modeling of the FiO_2, HR, and RR to SpO_2 dynamics in the presence of unfiltered noise for the purposes to creating a singular, general description model for control design.
- Design an adaptive model predictive controller that could regulate the SpO_2 without explicitly knowing the singular model a priori using the clinical best practices outlined in [5].

1.4 Thesis Overview

Chapter 2 discusses the polynomial system identification process. This process begins with data preprocessing, where an automated approach to finding SpO_2 recovery events for polynomial estimation is presented. From there, a brief overview of polynomial system identification modeling is introduced for two polynomial modeling structures:

autoregressive with exogenous inputs (ARX) and Box-Jenkins (BJ) models. To choose between these identified models, two metrics are introduced for model selection: Akaike's Information Criterion (AIC) and the sum of mean squared errors (ΣMSE). The best performing models, for both model structures, for each metric, are then compared in detail to determine a singular winning model for control design.

Chapter 3 introduces the AMPC methodology and different simulation results for the singular winning model. Chapter 3 begins with an overview of model predictive control (MPC) as well as a basic synopsis of the recursive polynomial ARX estimator. An additional a single static PI controller is designed to serve as a baseline comparison for the AMPC. Lastly, several simulations are performed using both controllers to assess the performance of the AMPC in the presence of both stressing step and periodic disturbances.

Chapter 4 contains a summary of the methods and results from the polynomial system identification, the adaptive model predictive controller, and gives some future recommendations.

2 Polynomial System Identification Modeling

2.1 Data Preprocessing

Data from eleven days was analyzed of premature infants with frequent desaturation events under nurse manual control. The data collected was FiO_2, HR, RR, and SpO_2. The FiO_2 was collected inline with the inspired oxygen supply, quantized to 0.1%, and sampled at every second. The HR, RR, and SpO_2 was collected every five seconds from a Masimo® pulse oximetry unit and quantized to 1 beat per minute (BPM), 1 breath per minute (BPM), and 1% for each respective channel. All data was recorded to a Labview® VI data acquisition system. Fig. 2-1 gives a representation of the sensor and data collection procedure. FiO_2 data was matched to the HR, RR, and SpO_2 through the data logging time stamps to keep a constant 5 second sampling rate. An example of an entire day, day 2, of collected SpO_2, FiO_2, HR, and RR data can be found in Fig. 2-2.

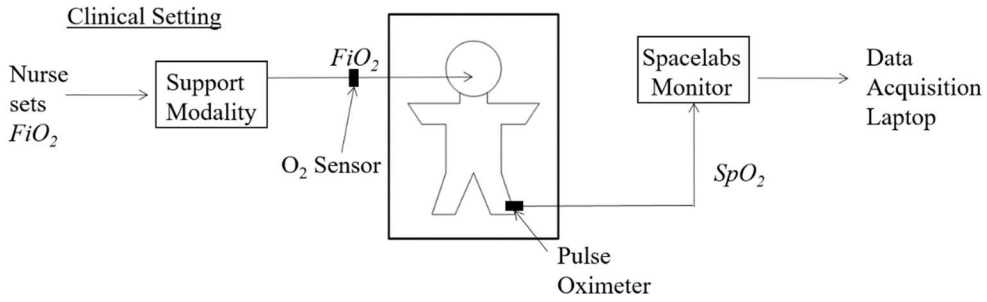

Fig. 2-1 Data collection setup [29].

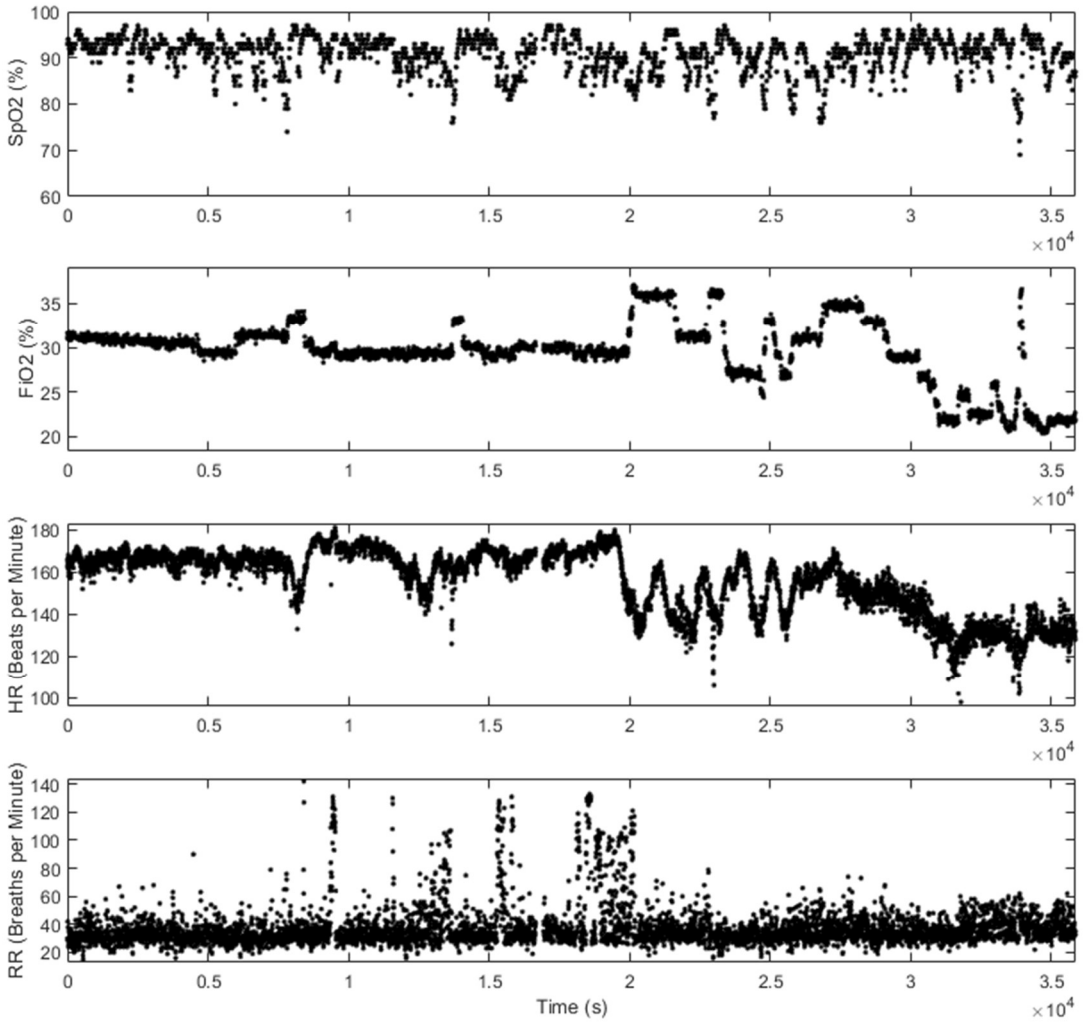

Fig. 2-2. An example of an entire day's worth of SpO_2, FiO_2, HR, and RR data.

The manual control action from the nurses, is categorized as step inputs. The step inputs were typically large positive FiO_2 adjustments, with less drastic negative weaning adjustments. Furthermore, it is assumed that the nurses are performing adjustments for the sole purpose of maintain SpO_2 target limits. To systematically find major FiO_2 adjustments, the derivative of the FiO_2 measurements were calculated using forward difference methods [32] over a day's worth of data. A major FiO_2 adjustment, also referred to as an event trigger, is defined as a derivative that is five times larger than the

standard deviation of the FiO_2 derivative for that day. Both positive and negative FiO_2 adjustments were considered event triggers as it had been shown that the FiO_2 to SpO_2 relationship cannot be determined by the positive adjustments alone [18].

Additionally, these step inputs from the manual control were not assumed to have settled before the next event trigger. As a result, to attempt to capture the entire system's reaction to a culmination of step input adjustments, an expanding time window was used. This window would start at the first event trigger and take the next N data samples. An example of the FiO_2 and the FiO_2 forward difference derivative can be found in Fig. 2-3. If no other event triggers are found within that N sample window, then the event is assumed to have concluded. If another event trigger is found within the sample window, then the entire window is extended to include an additional N samples.

The sample window size, N, was set to 78 samples for traversing the derivative response. This window sample size was determined by taking the mean time constant, 48s, plus two standard deviations, 26s, from the clustering used by [17] to predict the most of first order FiO_2 to SpO_2 responses (24%), thus resulting in a time constant of 97s. This time constant was also in line with the largest time constants found from [29], [31]. From this first order time constant, assuming a multiplier of 4 to reach steady state from a first order transfer function response, then divided by the sampling time of five seconds lead to the window size of 78 samples. The true minimum amount of data samples per event was 80, as the forward differencing method required that the first and last data point before the differencing transpired to be appended back onto the ends of the points found from the derivative event trigger samples.

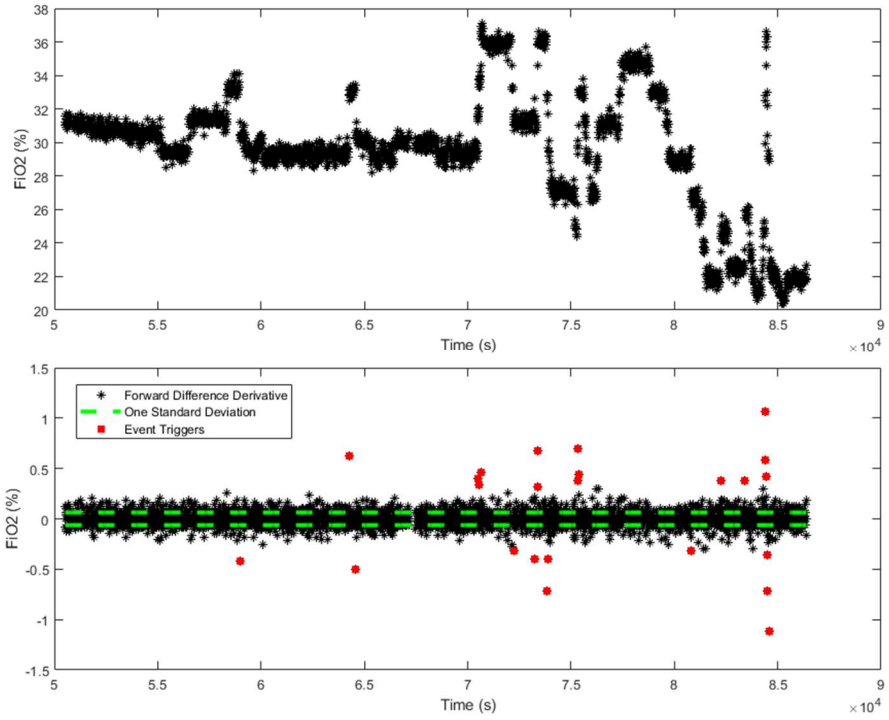

Fig. 2-3 Example of the FiO_2 event trigger investigation on the Day 2 data.

While it is desired to not explicitly prefilter the data, it is none the less required that a strong signal to noise ratio (SNR) be enforced to give the system identification methods the strongest chance of success. The signal to noise ratio is given by Eq. (2.1), where E is the expected value of a signal δ having random noise γ.

$$SNR = \frac{E[\delta^2]}{E[\gamma^2]} \tag{2.1}$$

Using the assumptions of an expected zero mean noise, and positive definite signals, Eq (2.1) can be reduced to Eq. (2.2) where μ_{sig} is the signal mean and σ_{sig} is the signal standard deviation.

$$SNR = \frac{\mu_{sig}}{\sigma_{sig}} \tag{2.2}$$

If all four signals, FiO_2, HR, RR, and SpO_2 do not meet the SNR minimum, the event was excluded from the available data set estimation pool.

Through trial and error, a signal to noise ratio of 4.5 was chosen. A table of the remaining events, the number of samples within each event, and the SNR of each event's signal are given in Table 2-1. More detailed information on the characteristics of the signals for the FiO_2, HR, RR, and SpO_2 given in Table 2-2, Table 2-3, Table 2-4, and Table 2-5 respectively. Picking the SNR involved the competing objectives of obtaining higher SNR while retaining sufficient data sets and number of different days with a data set available for estimation. It should be noted that a SNR of 3 would allow all days to be represented but would have allowed much noisier estimation data. The limiting factor was the RR signals, which often possessed significantly worse SNR than the other signals; as seen by the average SNRs in Table 2-1. While final choice of a minimum required SNR of 4.5 did none the less exclude three of the eleven days; a sufficient representation of differing days remained for making the overarching singular model system identification claim. An example of one of the remaining events, 2.1, can be found in Fig. 2-4.

Table 2-1 Summary of Events

Day	Event Name	Number of Samples in Event	Signal to Noise Ratio (SNR)			
			FiO_2	HR	RR	SpO_2
1	1.1	86	12.3	18.4	4.6	8.6
2	2.1	92	13.1	42.9	7.0	59.5
	2.2	92	16.9	20.6	4.6	18.4
	2.3	118	5.1	15.8	5.0	13.1
3	3.1	149	6.8	31.9	4.7	17.0
	3.2	101	15.8	37.8	4.7	53.8
4	4.1	80	90.2	22.1	6.2	24.2
	4.2	80	86.9	34.5	5.1	26.5
7	7.1	93	16.3	17.6	5.0	13.9
	7.2	157	5.2	7.9	4.6	12.9
	7.3	110	10.7	6.5	5.4	11.6
	7.4	81	26.8	21.5	5.8	10.2
9	9.1	116	30.6	61.6	4.6	23.9
	9.2	80	49.7	13.7	4.9	21.0
	9.3	80	32.3	43.4	5.2	25.7
10	10.1	81	29.7	113.3	4.5	36.7
11	11.1	80	34.0	40.3	6.1	76.6
	11.2	124	12.2	19.8	4.8	60.0
	11.3	80	33.9	20.8	4.6	62.7
Mean		99	27.8	31.1	5.1	30.3

Table 2-2 Event FiO_2 Characteristics

Day	Event Name	Max	Min	Mean
1	1.1	31.0	21.3	29.2
2	2.1	36.1	26.3	28.5
	2.2	33.8	24.4	31.7
	2.3	36.6	21.3	25.5
3	3.1	32.0	20.8	24.9
	3.2	32.5	24.7	26.3
4	4.1	77.2	71.4	76.4
	4.2	73.3	67.6	72.5
7	7.1	28.7	22.1	22.9
	7.2	43.1	27.4	32.8
	7.3	28.6	20.9	22.6
	7.4	27.4	21.2	26.7
9	9.1	42.9	38.0	40.2
	9.2	45.2	39.7	40.2
	9.3	50.6	40.1	49.6
10	10.1	51.7	41.2	42.9
11	11.1	38.5	31.2	32.2
	11.2	36.9	26.0	28.2
	11.3	31.0	26.2	27.7
Mean		40.9	32.2	35.8

Table 2-3 Event HR Characteristics

Day	Event Name	Max	Min	Mean
1	1.1	169	117	159
2	2.1	162	147	155
	2.2	166	139	157
	2.3	145	103	130
3	3.1	147	121	132
	3.2	151	130	137
4	4.1	165	135	151
	4.2	157	138	148
7	7.1	158	76	148
	7.2	196	63	160
	7.3	165	57	157
	7.4	167	134	156
9	9.1	148	137	142
	9.2	172	80	150
	9.3	159	139	157
10	10.1	155	150	153
11	11.1	159	130	151
	11.2	188	144	162
	11.3	156	114	149
Mean		162	119	150

Table 2-4 Event RR Characteristics

Day	Event Name	Max	Min	Mean
1	1.1	94	29	62
2	2.1	44	22	31
	2.2	55	20	33
	2.3	62	22	41
3	3.1	72	23	45
	3.2	71	27	42
4	4.1	96	43	69
	4.2	101	29	69
7	7.1	54	20	31
	7.2	103	25	64
	7.3	86	35	49
	7.4	94	45	62
9	9.1	91	27	58
	9.2	102	44	66
	9.3	64	27	45
10	10.1	102	32	65
11	11.1	64	32	45
	11.2	88	33	50
	11.3	109	33	44
Mean		82	30	51

Table 2-5 Event SpO_2 Characteristics

Day	Event Name	Max	Min	Mean
1	1.1	95	65	87
2	2.1	97	91	94
	2.2	94	79	88
	2.3	97	69	91
3	3.1	96	75	89
	3.2	95	89	92
4	4.1	98	83	95
	4.2	98	87	94
7	7.1	99	80	89
	7.2	99	71	91
	7.3	96	65	88
	7.4	97	63	91
9	9.1	95	81	90
	9.2	93	77	85
	9.3	84	72	76
10	10.1	94	86	90
11	11.1	98	93	96
	11.2	98	88	95
	11.3	96	90	94
Mean		96	79	90

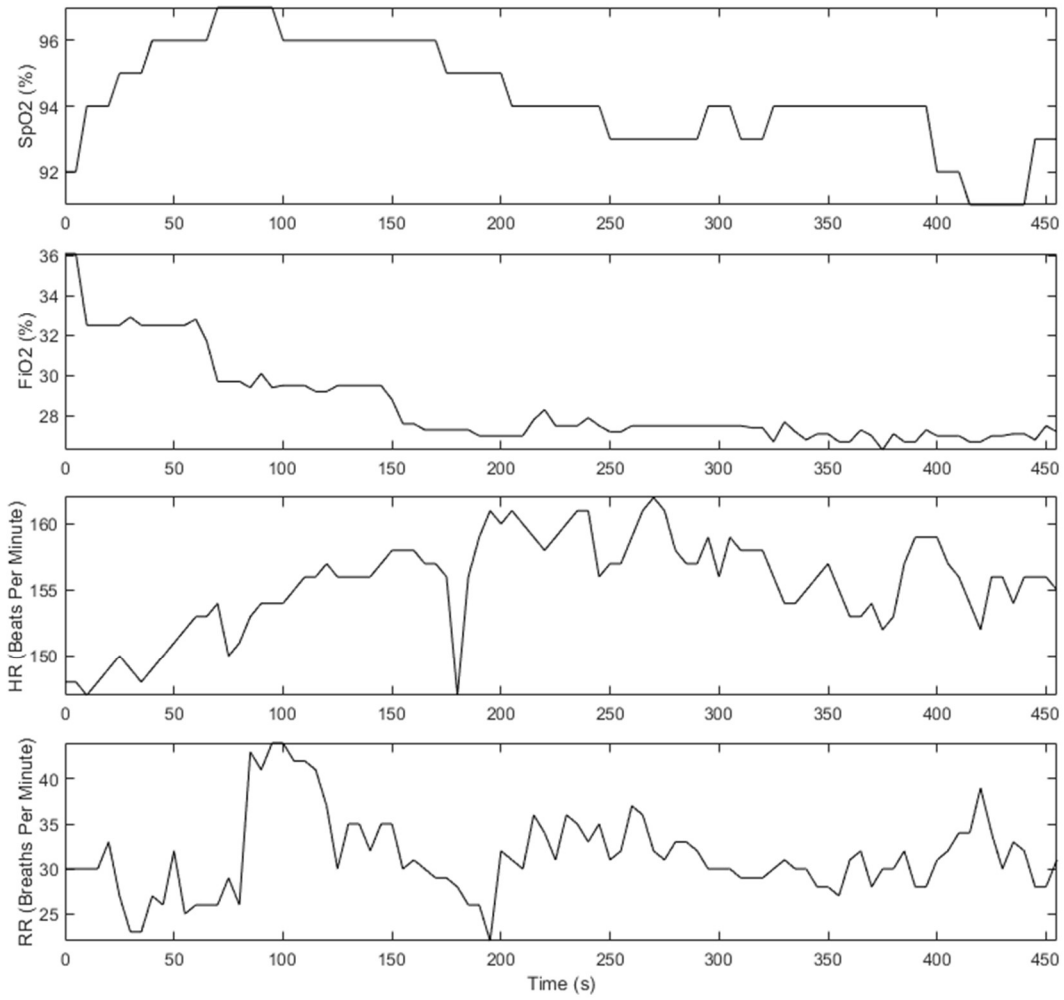

Fig. 2-4 The SpO_2, FiO_2, HR and RR time data for event 2.1

Examining Table 2-2, it can be seen that most of the FiO_2 levels were typically on the lower end of the spectrum, nearer room oxygen levels, except for day four. Day four has mean FiO_2 levels that are near double the mean of the other days, 74.5% versus 35.8%. This day was none the less kept in order to also model the effects of higher FiO_2 levels on the dynamics of the neonate. Both Table 2-3 and Table 2-4 summarize the characteristics of the HR and RR measurements of the events. Items of note from Table 2-5 is that manual control events only kept the mean of the SpO_2 within the 87-93% range in only eleven of the events, or only 57.9% of the time. Another observation is that

the minimum SpO_2 for the collection of events is below 87% for only fourteen of the events. This could be explained by the possibility that those days had higher target rates than the 87-93% SpO_2 target rate. Overall, the events found in Table 2-1 are deemed a reasonable representation of the neonatal population, and sufficient for modeling.

To prepare for both model estimation and validation, the event sets had to be binned into either a training or validation data set. This was done by randomly assigning fifteen data sets to train, and the remaining four to the validation data set. The training set would be explicitly used in the iterative fitting of the polynomial models. The validation data set served as a check on the possible noise overfitting and serve as a method of quantifying the generalization of the model fitting process. It would also be used as a component in the sum of mean squared error model metrics. Table 2-6 shows which events were sorted into either category.

Table 2-6 Training and Validation Data Set Sorting

Training Data	Validation Data
1.1	3.2
2.1	7.4
2.2	9.1
2.3	11.1
3.1	
4.1	
4.2	
7.1	
7.2	
7.3	
9.2	
9.3	
10.1	
11.2	
11.3	

2.2 System Identification Background for Time-Invariant Linear Systems

A linear, time-invariant, causal multi-input, single output (MISO) discrete system response is defined by Eq. (2.3), where y is the system response, t is the time, u is a

deterministic input, n_u is the total number of inputs, and g is the polynomial impulse response per input u [35].

$$\mathrm{y}(t) = \sum_{i=1}^{n_u} \sum_{k=1}^{\infty} g_i(k) u_i(t-j), \qquad t = 0,1,2,\ldots \tag{2.3}$$

The time, t, is given in terms of Eq. (2.4) where k is the sampling instant and T is the sampling rate.

$$\mathrm{t} = \mathrm{kT} \qquad k = 0,1,2,\ldots \tag{2.4}$$

In actual, real world situations, noise is present, and can be lumped together into the linear framework of Eq. (2.3) by including an additive term, *v(t)*, resulting in Eq. (2.5).

$$\mathrm{y}(t) = \sum_{i=1}^{n_u} \sum_{k=1}^{\infty} g_i(k) u_i(t-k) + v(t), \qquad t = 0,1,2,\ldots \tag{2.5}$$

This disturbance can be approximated by past disturbance impulse responses given by Eq. (2.6), where h is the polynomial impulse response to a white noise probability distribution disturbance input e.

$$\mathrm{v}(t) = \sum_{k=1}^{\infty} h(k) e(t-k), \qquad t = 0,1,2,\ldots \tag{2.6}$$

While the description given in Eq. (2.6) "does not allow completely general characterizations of all possible probabilistic disturbances, it is versatile enough for most practical purposes [35]." A common shorthand used in system identification is the backwards shift operator q, defined by Eq. (2.7).

$$\mathrm{q}^{-1}\mathrm{u}(t) = u(t-1) \tag{2.7}$$

Putting Eq. (2.6) into Eq. (2.5) for *v(t)* and substituting the backwards shift operator results for the general model given in Eq. (2.8) where *G(q)* is defined by Eq. (2.9) and *H(q)* is defined by Eq. (2.10).

$$\mathrm{y}(t) \;=\; G(q)u(t) \;+\; H(q)e(t) \tag{2.8}$$

$$\mathrm{G(q)} = \sum_{i\ =1}^{n_u} \sum_{k\ =\ 1}^{\infty} g_i(k) q^{-k} \tag{2.9}$$

$$\mathrm{H(q)} = 1 + \sum_{k\ =\ 1}^{\infty} h(k) q^{-k} \tag{2.10}$$

Equations (2.9) and (2.10) relate to the z-transform as seen in Eq. (2.11) and (2.12).

$$\mathrm{G(z)} = \sum_{i\ =1}^{n_u} \sum_{k\ =\ 1}^{\infty} g_i(k) z^{-k} \tag{2.11}$$

$$\mathrm{H(z)} = 1 + \sum_{k\ =\ 1}^{\infty} h(k) z^{-k} \tag{2.12}$$

2.3 Models of Linear Time-Invariant Systems

2.3.1 Autoregressive with Exogenous Inputs Model

There are many common methodologies to carry out the black-box parameterization of Eq. (2.8); with the most immediate being the autoregressive with exogenous inputs (ARX) model given by Eq. (2.14) where ***B****(q)* is the zeros of the inputs, ***A****(q)* is the shared dynamic poles, and *K* is the input to output delay.

$$y(t) = \sum_{i\ =\ 1}^{nu} \frac{\boldsymbol{B}_i(q)}{\boldsymbol{A}(q)} u_i(t\ -\ K) + \frac{1}{\boldsymbol{A}(q)} e(t) \tag{2.13}$$

The main strength of an ARX model is that it is a linear regression system [35], allowing for efficient, non-iterative solutions. This property was later utilized in section 3.1.1

where the linear least squared property was used to recursively estimate a model in real time. The model structure of an ARX model for a single input is given by Fig. 2-5.

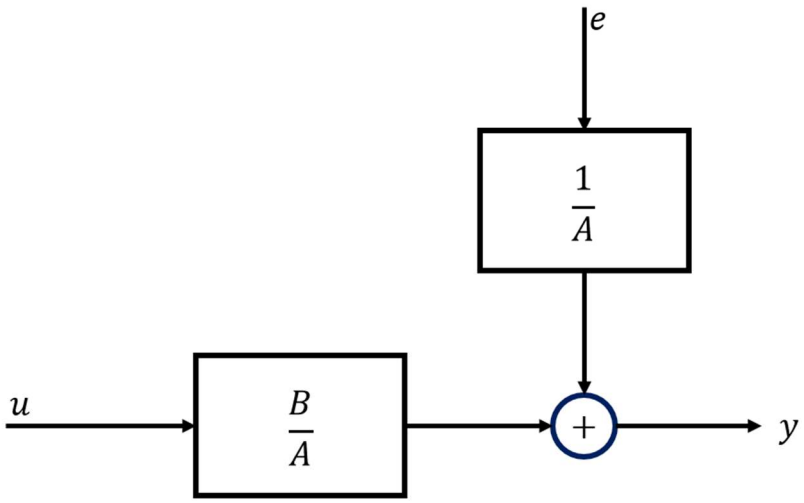

Fig. 2-5. The ARX Model Structure, redrawn from [35]

2.3.2 Box-Jenkins Model

An issue with the ARX model is that there is shared dynamics between the noise and the deterministic inputs. For modeling the neonate respiratory system, it was desired to be able to separate out the noise as it was believed to be possible unknown dynamics of the system. This led to the investigation of the more flexible Box-Jenkins (BJ) model shown by Eq. (2.14).

$$y(t) = \sum_{i=1}^{nu} \frac{\boldsymbol{B}_i(q)}{\boldsymbol{F}_i(q)} u_i(t - K) + \frac{\boldsymbol{C}(q)}{\boldsymbol{D}(q)} e(t) \tag{2.14}$$

A BJ model is a model of a deterministic polynomial model from known inputs, ***B****(q)* and ***F****(q)*, as well as a "colored noise" model, polynomial ***C****(q)* and ***D****(q)*. The BJ model structure for a single input is shown in Fig. 2-6. The major drawback of the BJ model is that it is a nonlinear regression, which means that it must be solved iteratively [35].

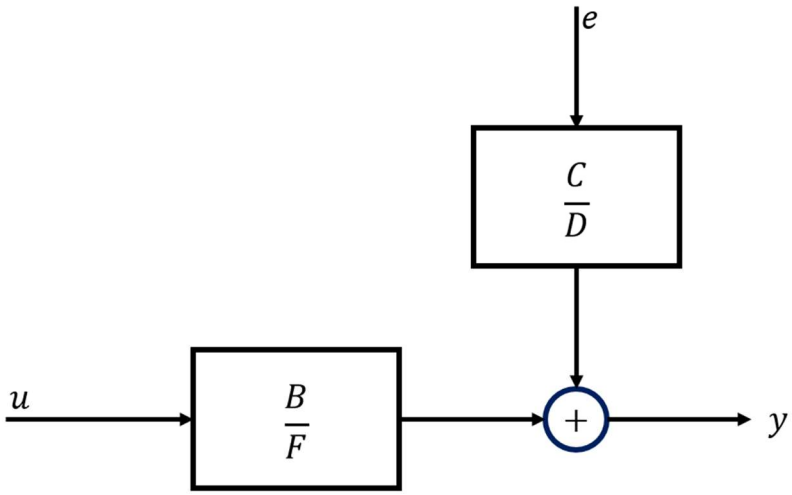

Fig. 2-6. The BJ-model structure, redrawn from [35]

2.3.3 Polynomial Model Estimation Settings

As both the ARX model and the BJ model polynomial parameters are solved through either a linear regression or nonlinear iterative processes, the main parameter open to investigation to the user is model order, also known as the number of regression free parameters. To thoroughly, and efficiently, examine such a large design space, a parameter sweep of all possible combinations of settings for the poles, zeros, and delays was investigated for both the ARX and BJ model structure. Table 2-7 gives the parametric sweep settings for the ARX model while Table 2-8 gives the BJ parametric sweep settings. A parameter sweep method was chosen due to the very black-box nature of the neonatal. There is a high chance that of unmodeled or unknown dynamics. In addition, a parameter sweep methodology fits well into the integer programming problem that is selecting model order.

Table 2-7 ARX Parameter Sweep Settings

Input	Minimum B(q) Order	Maximum B(q) Order	Minimum A(q) Order	Maximum A(q) Order	Minimum Delay K	Maximum Delay K
FiO_2	1	1	1	2	1	12
HR	1	1	1	2	1	12
RR	1	1	1	2	1	12

Table 2-8 BJ Parameter Sweep Settings

Input	Minimum B(q) Order	Maximum B(q) Order	Minimum F(q) Order	Maximum F(q) Order	Minimum Delay K	Maximum Delay K
FiO_2	1	1	1	2	1	12
HR	1	1	1	2	1	12
RR	1	1	1	2	1	12

Disturbance settings for the ARX model polynomial A(q) was be allowed to be between first and second order. The disturbance on the BJ model C(q) and D(q) were fixed to C(q) = 1 and D(q) = 2, respectively. This was done to expand noise modeling flexibility of possible unknown dynamics. From these settings, it can be seen that each G(q) transfer function is allowed to take on as simple of a model as a gain and time constant first order model, such as those found by [17], [26], [29], all the way to a one zero, two pole, and a twelve sample delay.

For the solvers of the polynomial models, the main loss function is given by Eq. (2.15), where ε are the prediction errors.

$$\varepsilon(t) = y_{measured} - \mathrm{G(q)}u_{measured}(t) \quad (2.15)$$

An added step for the BJ model involves estimating H(q). This is done by fixing G(q) from Eq. (2.15) and finding the H(q) that minimizes the one step ahead prediction error given by Eq. (2.16) where $\hat{y}$ is the predicted system response.

$$y(t) - \hat{y}(t|t-1) = -H^{-1}(q)G(q)u(t) + H^{-1}(q)y(t) \quad (2.16)$$

Additional solver settings and data preprocessing include removing the means from each individual event signal, setting initial conditions, setting additional constraints, and setting the nonlinear solver for the BJ model. Removing the means from each individual event signal was performed as it would allow for the removal of explicit bias within the data. The state initial conditions were set to be "backcast," which is estimating the initial conditions on a least square fit. Initial conditions must be estimated as all these events do not happen from a steady state initial condition. The estimated models were restricted to stable systems, as it is assumed that the neonate system is a stable system. Polynomial orders were restricted to be strictly proper once transformed into the z domain. The DC gain of the FiO_2 to SpO_2 must be positive definite, evidenced by the gains of the first order transfer functions found in [17], [29]. The BJ nonlinear solver was set to automatic initialization. This means that it will pick between Subspace Gauss-Newton least squares, Adaptive Gauss-Newton search, Levenberg-Marquardt Least Squares Search, and Steepest Decent with the first method leads to a reduction in the estimation cost being chosen [36]. Lastly, the maximum number of iterations for the nonlinear solvers to run was one thousand iterations. This was chosen from trial and error to show reasonable convergence with higher order models and overall compute time.

2.3.4 Model Selection Criteria

Two different scalar objectives were investigated for picking a singular winning model from all the parameter sweep estimated models. The two metrics was the Akaike's Raw Information Criterion AIC and the model that produced the smallest sum of squared error (ΣMSE) across both the training and validation data. Akaike's Raw Information Criterion gives a method of dealing with the competing objectives of having the smallest model order size, while also getting strong one step ahead prediction abilities [35], [37]. It is designed to penalize unnecessarily higher order models. Therefore, the best model is the model that has the smallest AIC [38]. Equation (2.17) gives the Akaike's Raw Information Criterion where $\boldsymbol{\theta_N}$ is the estimated parameters, and n_p is the number of estimated parameters.

$$AIC = N * log\left(det\left(\frac{1}{N} \sum_{1}^{N} \epsilon\left(t, \hat{\theta}_N\right) \left(\epsilon\left(t, \hat{\theta}_N\right) \right)^T \right) \right) + 2n_p + N * (log(2\pi) + 1) \quad (2.17)$$

The secondary metric for picking the winning model is the ΣMSE. The ΣMSE is defined by Eq. (2.18) where N_s is the number of data sets.

$$\Sigma MSE = \sum_{j=1}^{N_s} \frac{1}{N} \sum_{i=1}^{N} (y_i - \hat{y}_i)^2 \quad (2.18)$$

The number of data sets is nineteen, or all the training and validation data sets. The choice for using this statistic came from a desire to see the model that could most accurately predict all nineteen data sets. Furthermore, evaluating the MSE across all the data sets allowed for an additional method for comparing performance of the model selected from AIC. Calculating the ΣMSE once again does require the estimation of the initial states of the models.

2.4 Model Results and Analysis

From the parameter sweep settings discussed in 2.3.3, a total of 3,456 ARX models and 13,176 BJ models were estimated from the collection of training data sets given in Table 2-6. The summary of the ARX and BJ parameter sweep results are given in Table 2-9. As can be seen from Table 2-9, the mean AIC between both the ARX and the BJ model structures was similar, yet the standard deviation for the BJ models was an order of magnitude larger than the standard deviation for the ARX model structure. Furthermore, it is shown that the mean ΣMSE was significantly lower for the BJ model structure than the ARX, but also had a significantly larger standard deviation. The main takeaway from Table 2-9 is that the AIC, the metric that is designed to discourage unnecessary higher order modeling was the same between both model structures, while the ΣMSE was on average lower for the BJ. This lends to the conclusion, that while the standard deviation, and thus the statistical spread of the modeling metric of the BJ model structure is higher, it has the better chance of producing a better overall model.

Table 2-9 Model structure parameter sweep metric results

Model Structure	Mean ΣMSE (Std)	Mean AIC (Std)
ARX	260.6 (12.3)	5064.6 (29.9)
BJ	107.8 (432.0)	5061.7 (254.3)

From both model structures, the models that produced the smallest ΣMSE and the smallest AIC were extracted, now referred to as the winning models. For the ARX models, the winning AIC and ΣMSE model polynomial orders are given in Table 2-10 and Table 2-11 respectively. The BJ polynomial orders for the models that minimized the

AIC and the ΣMSE are given in Table 2-12 and Table 2-13 respectively. What can be seen from the polynomial order tables is that there is a consistent need to increase the order for the RR and a need to have a delay for the FiO_2. Yet it appears that the FiO_2 can still be modeled effectively by a simple delay, gain, and time constant model. Furthermore, it is seen that the FiO_2 and HR for all, but the minimum AIC BJ model, are same. The minimum AIC BJ on the other hand found that a shorter delay on the FiO_2 and a longer delay on the HR was necessary.

Table 2-10 Minimum AIC ARX Model Polynomial Orders

Input	B(q)	Delay
FiO_2	1	5
HR	1	1
RR	2	3
A(q) = 1		

Table 2-11 Minimum ΣMSE ARX Model Polynomial Orders

Input	B(q)	Delay
FiO_2	1	5
HR	1	1
RR	2	1
A(q) = 1		

Table 2-12 Minimum AIC BJ Model Polynomial Orders

Input	B(q)	F(q)	Delay
FiO_2	1	1	2
HR	1	2	9
RR	1	1	1

Table 2-13 Minimum ΣMSE BJ Model Polynomial Orders

Input	B(q)	F(q)	Delay
FiO_2	1	1	5
HR	1	2	1
RR	1	2	2

A major observation of the winning models is that the highest possible order combinations are not present. The highest order model would be if two poles were selected for either A(q) in the ARX models or for all of F(q) in the BJ models. Yet, there might still be a need to investigate additional higher order models for the HR and RR systems for the BJ models.

To further the objective of picking a singular model for control design, the unit step response of G(q) for each of the winning models was plotted and given in Fig. 2-7. DC gains for G(q) of the winning models are given in Table 2-14. From the DC gains of G(q), it is seen that the HR and RR both have a smaller DC gain than the FiO_2, with the DC gain of the RR is approaching or at zero. Additionally, negative dc gain for the HR to SpO_2 response on the minimum AIC BJ model is an interesting phenomenon which is

explainable as the minimum AIC BJ model also has the large 9 sample delay for the HR. All of these ranges are consistent with those found by [29].

Table 2-14 DC Gain, SpO_2 (%), of G(q) for Winning Models

Model		FiO_2	HR	RR
ARX	**Min AIC**	1.2	0.4	0.1
	Min ΣMSE	1.2	0.4	0
BJ	**Min AIC**	1.6	-0.4	0.1
	Min ΣMSE	0.6	0.1	0.1

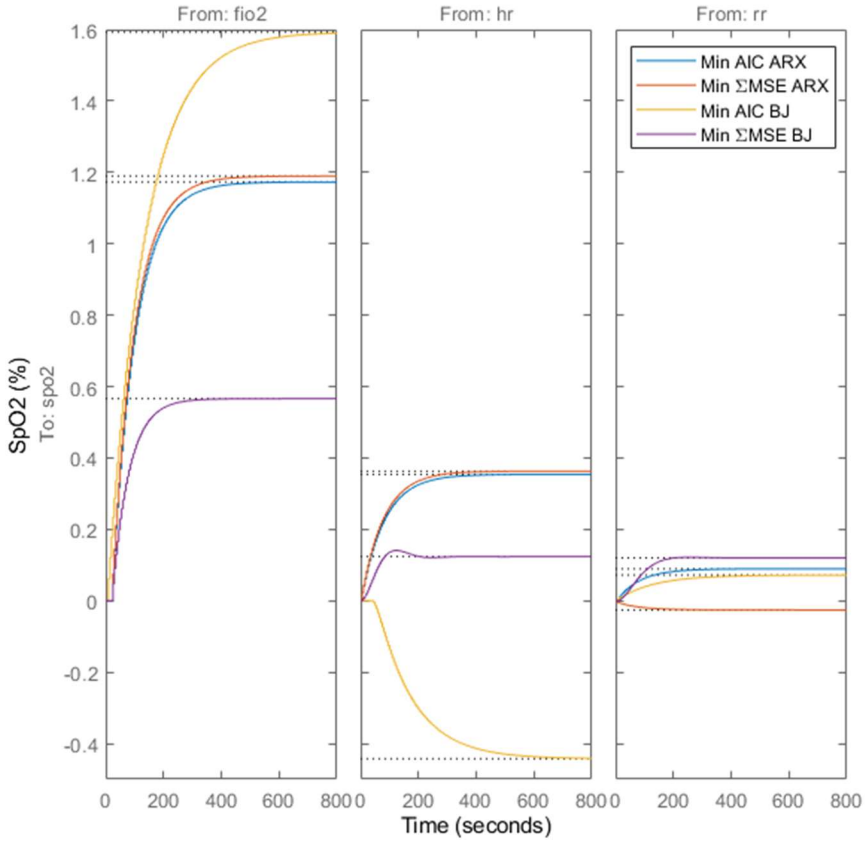

Fig. 2-7 G(q) Unit Step Response for Winner Models

Yet, the real story of what separates the four winning models can be found in examining the stochastic disturbance model, H(q). The unit step responses for H(q) is given in Fig. 2-8 and the DC gains of H(q) given in Table 2-15. There it can be very clearly seen that the estimated stochastic disturbance models for all, but the minimum AIC BJ model, has dc gains that are significantly larger than the DC gains found in Table 2-14. This translates to a statement that most of the modeling of the SpO_2 is either unknown dynamics or noise. Therefore, maintaining the SpO_2 with the target limits would be physically impossible, which is obviously an unrealistic model. It should be noted that the peak value of the minimum AIC BJ model to a unit step response is 3.7%, which is much more reasonable.

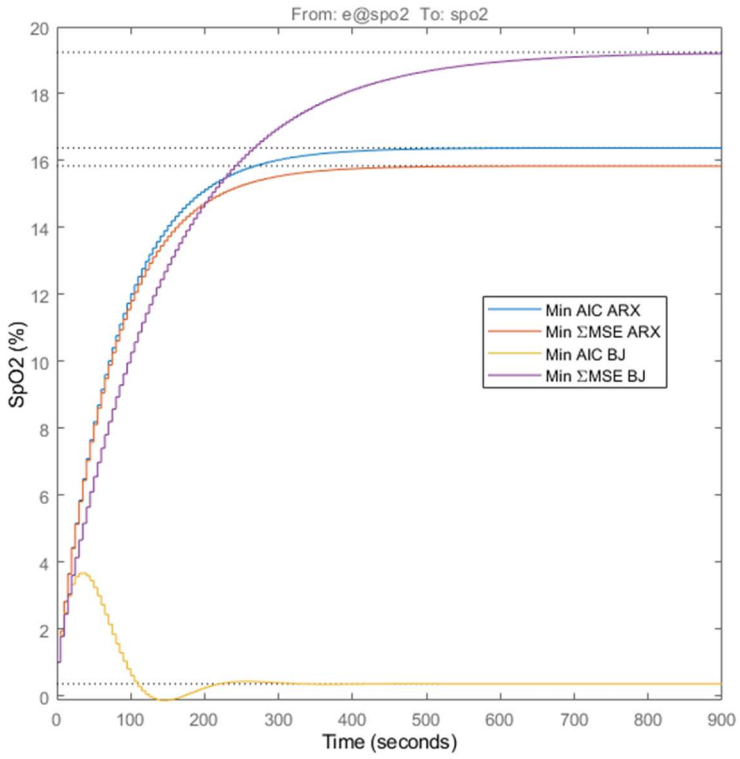

Fig. 2-8 H(q) Unit Step Response for Winner Models

Table 2-15 DC Gain, SpO_2 (%), of H(q) for Winning Models

Model		$eSpO_2$ (%)
ARX	**Min AIC**	16.4
	Min ΣMSE	15.8
BJ	**Min AIC**	0.4
	Min ΣMSE	19.2

A final model verification involves stimulating the models against the validation clinical input and output measurements and can be seen in Fig. 2-9. This simulation involved reintroducing the input and output means as well as estimating the initial conditions that would produce the least prediction error. This is needed as the events do not begin at steady state. In addition, no noise is being simulated. It can be very clearly seen that the BJ models produced the best simulation match. The MSE of the four winning models to the validation data events is given in Table 2-16. While the BJ models could more accurately simulate the neonate response over the entire event, the ARX models could reasonably simulate for a short period of time.

Table 2-16 MSE of Winning Models To Validation Data

Day	**ARX**		**BJ**	
	Min AIC	Min ΣMSE	Min AIC	Min ΣMSE
3.2	1.5	1.5	0.6	0.6
7.4	29.5	29.2	0.7	0.6
9.1	5.9	6.1	2.1	2
11.1	2.1	2.0	0.6	0.6
Σ	39.0	38.8	4.0	3.8

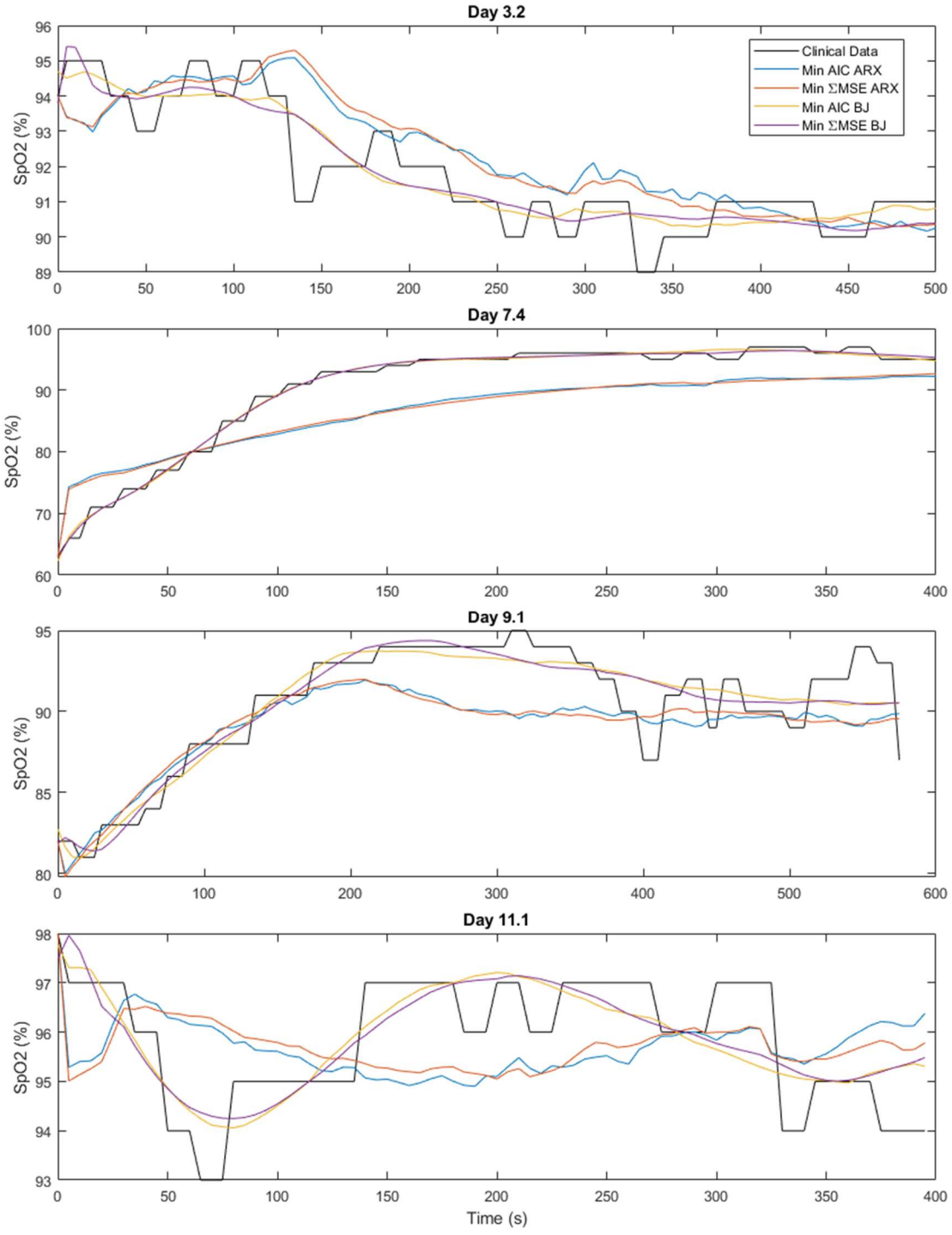

Fig. 2-9 Simulation Of Winning Models on Validation Data Sets

When all these results are considered, the singular winning model that is carried forward is the minimum AIC BJ model. The minimum AIC BJ model not only scored the lowest AIC, but near the same ΣMSE that the minimum ΣMSE model produced on the validation data. In addition, the minimum AIC BJ model had the smallest H(q) response, meaning that it was able to minimize Eq. (2.15) by explain the dynamics the most with G(q). Thus, it will be the only model carried forward for control design and simulation. Thusly, the minimum AIC BJ model will be referred to as "the neonate model" and any reference to G(q) and H(q) will be about the minimum AIC BJ model. Full discrete time transfer functions of the four models can be found in Appendix A: Winning Identified Models.

3 Adaptive Model Predictive Control

3.1 Adaptive Model Predictive Controller Synthesis

3.1.1 Model Predictive Control

The choice to go with a model predictive controller (MPC), and the resulting Adaptive Model Predictive Control (AMPC) stemmed from the research objective to implement best practices [5]:

- Avoid frequent "up and down and up again" FiO_2 adjustments
- SpO_2 is to be maintained at a minimum saturation of 87%
- FiO2 should be weaned off at 2-5% if above 93%
- FiO_2 should be never increase by more than 5%

While these best practices have proven successful in clinical testing, this field continues to evolve, with the best practices and target ranges for SpO_2 still undecided [8]. Yet, what can be taken away from these best practices is that they are often constraint formulation, which is the biggest advantage of an MPC architecture. An MPC controller can therefore explicitly implement the best practices, such as the best practice constraint of not increasing the FiO_2 by more than 5% per adjustment. In addition, it can perform range control to keep the output within the design objective of 87-93% SpO_2 [40].

The discrete time linear model for control of a MISO system can be expressed by Eq. (3.1) [41], where $\boldsymbol{x}$ are the internal states, $\boldsymbol{u}$ are the manipulated variables, $\boldsymbol{d}$ are the measured disturbance variables, $\boldsymbol{w}$ are independent gaussian state disturbances, $\boldsymbol{\xi}$ is independent gaussian noise, $\boldsymbol{A}$ is the internal state matrix, $\boldsymbol{B}_u$ is the input matrix for the measured variables, $\boldsymbol{B}_d$ is the input matrix for the disturbance variables, $\boldsymbol{C}$ is the output

matrix, $\boldsymbol{D}_u$ is the feedforward matrix for the inputs, $\boldsymbol{D}_d$ is the feedforward matrix for the measured disturbances, and y is the scalar output controlled variable.

$$\begin{aligned} \boldsymbol{x}(k+1) &= \boldsymbol{A}\boldsymbol{x}(k) + \boldsymbol{B}_{\boldsymbol{u}}\boldsymbol{u}(k) + \boldsymbol{B}_{\boldsymbol{d}}\boldsymbol{d}(k) + w(k) \\ y(k) &= \boldsymbol{C}\boldsymbol{x}(k) + \boldsymbol{D}_{\boldsymbol{u}}\boldsymbol{u}(k) + \boldsymbol{D}_d\boldsymbol{d}(k) + \xi(k) \end{aligned} \tag{3.1}$$

Both $w(k)$ and $\xi(k)$ are assumed to be zero mean and have parameter covariances given by Q_k and R_k. The initial values of Q_k and R_k are set to Eq. (3.2) and (3.3) respectively.

$$\boldsymbol{Q_0} = \boldsymbol{E}\left[[\boldsymbol{B_u B_d}][\boldsymbol{B_u B_d}]^{\boldsymbol{T}}\right] \tag{3.2}$$

$$\boldsymbol{R_0} = \boldsymbol{E}[\boldsymbol{D}\boldsymbol{D}^{\boldsymbol{T}}] \tag{3.3}$$

Model Predictive Control, sometimes referred to as receding horizon control, is an advanced control technique for satisfying inequality constraints. It is referred to as receding horizon control because while an entire sequence of control actions is calculated, only the next time step's is implemented before a new sampled measurement. With the new sampled measurement a new set of control sequences are calculated [40]. The basic concept of MPC is given in Fig. 3-1, where the concepts of both prediction horizon, *Ph* and the control horizon, *Mh*, are presented. The prediction horizon is the number of sampling instants that the MPC will be trying to control over, while the control horizon is how many control sampling instants are available for control. It is common to hold the control action constant after the k + Mh sampling instant [40].

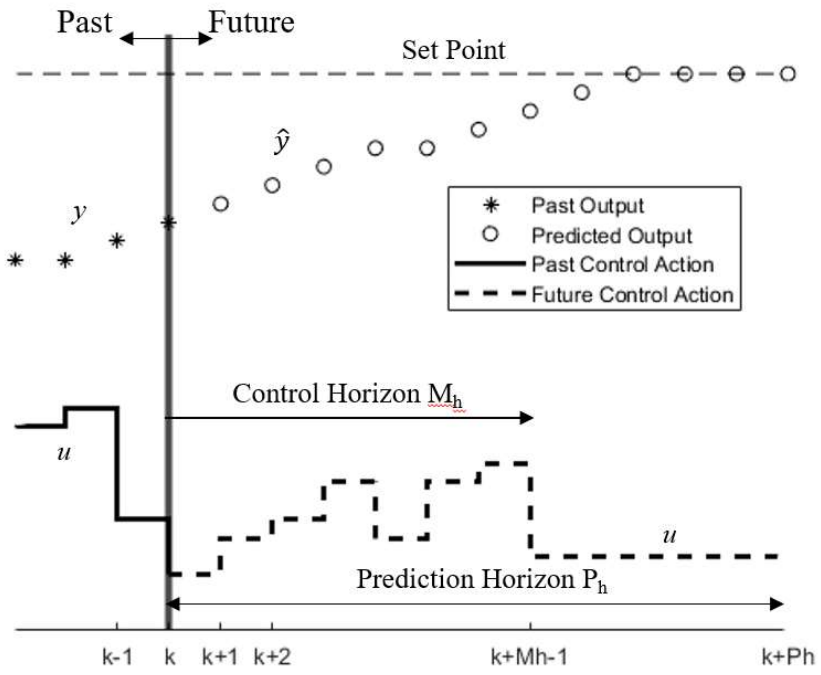

Fig. 3-1 Basic concept for MPC, recreated and modified from [40]

For the neonatal SpO_2 regulation application, the prediction horizon was set to 84 samples, which is the 80 samples used for estimating the minimum window size in section 2.1, and rounded to the nearest minute for a 5 second sample rate. As for the control horizon, that was set to be blocked to a control action every minute, or 12 sampling instants. This design decision once again came from the desire to take conservative FiO2 adjustments to keep in line with best practice. The concept of input blocking is a computational advantage where the manipulated variable is left constant across a block. An example of this can be found Fig. 3-2 where the manipulated variable is held constant over each block of three sampling instants starting at sampling instant k+4. The overall flow of MPC algorithmic flow given in Fig. 3-3. In Fig. 3-3, MV are the manipulated variables, DV are the disturbance variables, and CV are the controlled variables. The application for the control of the neonate model, would be setting the

manipulated variable to the FiO2, the disturbance variables to the HR and RR, and the controlled variable to the SpO2. The ill conditioning and local steady state optimization are left for the quadratic programming solver.

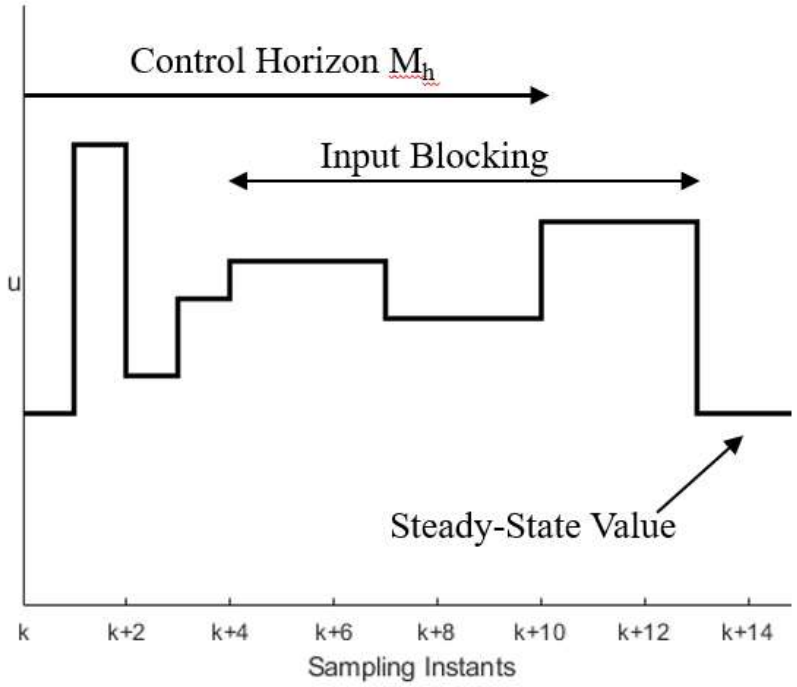

Fig. 3-2 Example of Input Blocking, recreated and modified from [15].

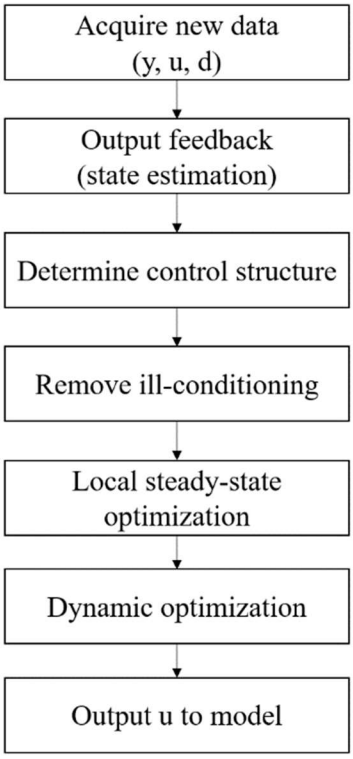

Fig. 3-3 Flow of MPC calculations at each control execution, recreated and modified from [41]

The internal model structure for the MPC was chosen to be three independent first order transfer functions found by [29]. A major goal of the AMPC is to be able to satisfactorily regulate the SpO_2 on an unknown model, especially if that unknown model is of higher order and with delay than its internal nominal model. Thus, Eq. (3.4) was the simplest known model to represent the dynamics of the neonate for at least a short period of time and real time control.

$$\mathrm{SpO}_2(s) = \frac{2.957}{145.9s\ +\ 1} FiO_2 + \frac{-0.07}{177.2s\ +\ 1} HR \frac{-0.8929}{151.3s\ +\ 1} RR \qquad (3.4)$$

The nominal model that is used for the AMPC initial internal model is the mean gain and time constant for the continuous time first order given in [29]. This model is converted into a discrete time state space model at a five second sampling rate for use in the AMPC.

For state estimation of the adaptive model predictive controller, a time varying Kalman filter was used, and it's basic algorithm given in Eq. (3.5) through Eq. (3.9) [42].

$$\boldsymbol{Pc}_k^- = \boldsymbol{A}_{k-1}\boldsymbol{P}_{k-1}^+\boldsymbol{A}_{k-1}^T + \boldsymbol{Q}_{\,k-1} \tag{3.5}$$

$$L_k = \boldsymbol{P}_{\boldsymbol{k}}^-\boldsymbol{C}_k^T(\boldsymbol{C}_k\boldsymbol{P}_{\boldsymbol{k}}^-\boldsymbol{C}_k^T + R_k)^{-1} \tag{3.6}$$

$$\hat{\boldsymbol{x}}_k^- = \boldsymbol{A}_{k-1}\hat{\boldsymbol{x}}_{k-1}^+ + \boldsymbol{B}_{k-1}\boldsymbol{u}_{k-1} \tag{3.7}$$

$$\hat{\boldsymbol{x}}_k^+ = \hat{\boldsymbol{x}}_k^- + L_k(y_k - C_k\hat{\boldsymbol{x}}_k^-) \tag{3.8}$$

$$\boldsymbol{Pc}_k^+ = (I - L_k\boldsymbol{C}_k)\boldsymbol{P}_k^- \tag{3.9}$$

In Eq. (3.5) through (3.9), $\boldsymbol{Pc}$ is the parameter covariance, $\hat{\mathbf{x}}$ is the estimate of the state $\boldsymbol{x}$, L is the Kalman filter gain, and the + and – superscripts denote the calculations a priori and posteriori the new measurement y.

The cost function for dynamic optimization is given by the quadratic programming cost function in Eq. (3.10) where J is the objective function, $\widehat{\boldsymbol{E}}$ is the prediction errors over the horizon, $\boldsymbol{u_h}$ are the next controller moves over the control horizon, α is the output variable weighing matrix, and β is input variable weighting matrix [40].

$$\min_{u_h(k)} \boldsymbol{J} = \widehat{\boldsymbol{E}}(k+1)^{\,T}\boldsymbol{\alpha}\widehat{\boldsymbol{E}}(k+1) + \boldsymbol{u_h}(k)^T\boldsymbol{\beta}\boldsymbol{u_h}(k) \tag{3.10}$$

As it is desired to be able to penalize the FiO_2 adjustment rates, an additional cost is added to Eq. (3.10) and given in Eq. (3.11) where ω is a weight on rate of change of the control variables, $\Delta\boldsymbol{u_h}$, over the horizon.

$$\min_{u_h(k)} \boldsymbol{J} = \widehat{\boldsymbol{E}}(k+1)^T \boldsymbol{\alpha} \widehat{\boldsymbol{E}}(k+1) + \boldsymbol{u_h}(k)^T \boldsymbol{\beta} \boldsymbol{u_h}(k) + \Delta \boldsymbol{u_h}(k) \boldsymbol{\omega} \Delta \boldsymbol{u_h}(k) \quad (3.11)$$

$\Delta \mathbf{u_h}$ for a single step is defined as shown in Eq. (3.12)

$$\Delta u_h(k) = u_h(k) - u_h(k-1) \quad (3.12)$$

α is set to 100, 1 for β, and 10,000 ω. This tuning was designed to create a conservative quadratic cost function that prioritizes less aggressive adjustments in the FiO_2 to keep in line with minimizing constant up and down FiO_2 adjustments [5].

Additionally, there are hard boundary constraints on both the manipulated variables and controlled variable. These inequality constraints are given by Eq. (3.13) through (3.15), where the *lb* and *ub* stand for the upper and lower bounds of the variables.

$$\boldsymbol{u_h}^{lb}(k) \leq \boldsymbol{u_h}(k+j) \leq \boldsymbol{u_h}^{ub} \quad j = 0,1,\ldots M-1 \quad (3.13)$$

$$\Delta \boldsymbol{u_h}^{lb}(k) \leq \Delta \boldsymbol{u_h}(k+j) \leq \Delta \boldsymbol{u_h}^{ub} \quad j = 0,1,\ldots M-1 \quad (3.14)$$

$$y^{lb}(k+j) \leq \hat{y}(k+j) \leq y^{ub} \quad j = 0,1,\ldots M-1 \quad (3.15)$$

For this application, the hard inequality constraints on the manipulated variable, FiO_2, is between 21%, room oxygen levels [2], and 100%. The rate of change of the manipulated variable is set to upper and lower bounds of ±5% to keep in line with [5]. Lastly, the hard inequality constraint on the controlled variable, SpO_2 is set between 65% and 100%, the limits of the pulse oximeter.

An item done for computation implementation efficiency was that all the *u*, *d*, and *y* variables were scaled to be nondimensionalized between zero and one. This normalization was done by scaling the inputs by their spans. The spans were as follows:

the FiO_2 and SpO_2 were scaled between their hard inequality constraints while the HR and RR are scaled between their mean max and min from Table 2-3 and Table 2-4.

3.1.2 Recursive Polynomial Model Estimation

For the online model estimation necessary for the AMPC, a recursive polynomial model estimator was added. As real time estimation is a necessity, the ARX model structure was used, as it could be recursively estimated for MISO models and not be iterative solved like the BJ model. While the ARX model was shown to not accurately predict an entire event, it could at least perform well in the short term. The ARX model is recursively calculated at every sample time; thus, the drawback of being only able to accurately predict a short number of samples ahead only is minimized. The formula for a recursive least squares estimate is given in Eq. (3.16) and (3.17) where $\boldsymbol{\tau}$ is the parameter covariance of the least squared estimate, $\boldsymbol{\varphi}$ is a finite dimension of regression vectors, and λ is the forgetting factor [35].

$$\widehat{\boldsymbol{\theta}}_k = \widehat{\boldsymbol{\theta}}_{k-1} + \boldsymbol{\tau}^{-1}(k)\boldsymbol{\varphi}(k)\left[y(k) - \boldsymbol{\varphi}^T(k)\widehat{\boldsymbol{\theta}}_{k-1}\right] \tag{3.16}$$

$$\boldsymbol{\tau}(k) = \lambda(k)\tau(k-1) + \boldsymbol{\varphi}(k)\boldsymbol{\varphi}^T(k) \tag{3.17}$$

The equation for a forgetting factor is given in Eq. (3.18) [35], where T_0 is the number of most recent samples that are desired for estimation and λ is the forgetting factor.

$$T_0 = \frac{1}{1-\lambda} \tag{3.18}$$

Solving Eq. (3.18) for λ to results in Eq. (3.19), used to calculate the required forgetting factor.

$$\lambda = 1 - \frac{1}{T_0} \tag{3.19}$$

Keeping the last half an hour, or 360 samples at a 5 second sampling rate results in the forgetting factor of 0.9972. This window size allowed for enough data to be retained for estimation, while still allowing for the possible evolving dynamics of the neonate.

To facilitate a pure online estimation, no initial ARX model is given to the RPME, but instead a large initial parameter covariance, of 1e8 is used. Such a large parameter covariance biases the estimator to weight more to the measurements and less to the initial model [35]. Additionally, the size of the RPME ARX model was fixed to A(q) of third order, each B(q) to third order, and no internal delay. This is a result of the AMPC's internal state space model being the three independent first order transfer functions.

3.2 Tuned PI

A static PI controller is desired to baseline test the performance of the AMPC. In other words, it stemmed from the desire to investigate how well can the AMPC, not tuned on the higher order neonatal model, approaches or beats a static PI controller that was tuned specifically on said higher order model. As such, the PI controller can tune itself with the explicit knowledge of the noise spectrum within the model. The noise model was used to set an upper bound on the open loop gain for the purposes of not amplifying the noise. From the Bode diagram of the noise, shown in Fig. 3-4, it is seen that the point of 0dB magnitude is approximately 0.005 rad/s. This value was then set as target bandwidth frequency of the PI controller. This design objective, coupled with an additional design objective of 60 degrees of phase margin, resulted in a PI controller tuned through MATLAB's PID Tuner.

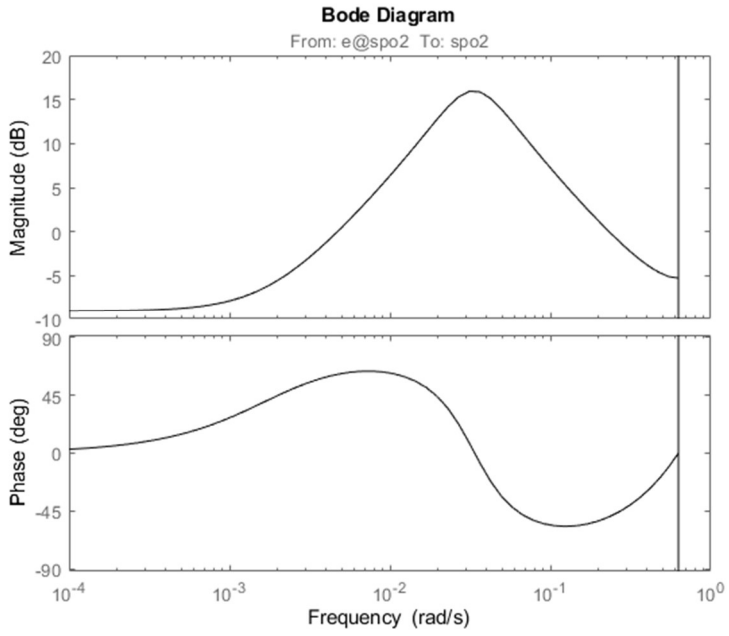

Fig. 3-4 Bode diagram of H(q)

3.3 Simulation and Results

A block diagram of the simulation environment is given in Fig. 3-5. It should be noted that in addition to the block diagram shown in Fig. 3-5, quantizers are placed into the measurement paths. That means that the HR, RR, and SpO_2 signals are all quantized to the nearest integer, while the FiO_2 measurement going into the RPME was quantized to the nearest 0.1 %. Initial conditions for the unit delays were all zeros, except for the initial condition for the FiO_2, which was found to work best with a nonzero initial condition. This was most likely due to the quantizers in the feedback paths. As a result, it was initialized to 1% FiO_2 off nominal. Nominal FiO_2, HR, RR, and SpO_2 are the mean of the means given in Table 2-2, Table 2-3, Table 2-4, Table 2-5. The value of 90%, the midpoint between 87% and 93% SpO_2 was the target reference point for both controllers. The SpO_2 had a saturation limit between 65% and 100%.

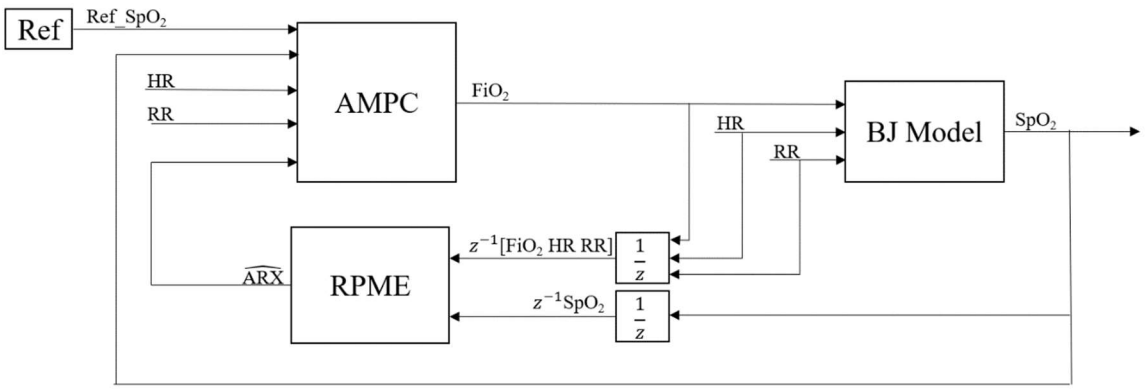

Fig. 3-5 Block diagram of AMPC, BJ Model, and RPME

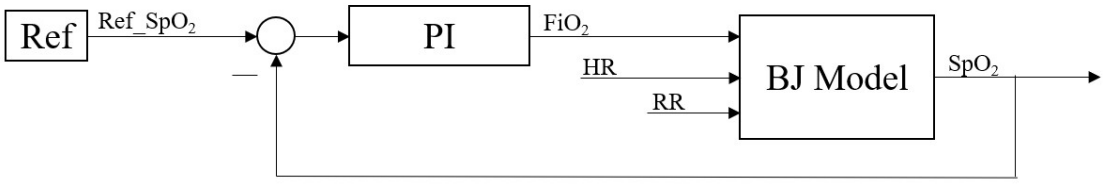

Fig. 3-6 Block diagram of the PI Controller and BJ Model

Two different sets of simulations were performed, both with and without the colored noise applied over the course of one hour of simulation time. The colored noise was turned off and on to compare an ideal response as well as the more realistic response with the unmeasured colored noise disturbance. All colored noise simulations used the same random number generator seed. The choice of one hour of simulation time was to show the continued stability and performance of the AMPC and RPME. As it was desired to stress the controllers, the measured disturbance on the HR and RR were both sent identical signals meant to cause a major desaturation, but opposite signs for the HR. The values of these signals were designed to stay within the mean of the max and min defined

by Table 2-3 and Table 2-4 for measured disturbance signal. All simulations compare the AMPC, PI, and zero FiO_2 control with 87% and 93% SpO_2 boundaries.

The first simulation was a major step desaturation. This desaturation event was designed by performing a negative step input of magnitude 30 after 10 minutes. The simulation results of the SpO_2 and the FiO_2 are given in Fig. 3-7. From Fig. 3-7, it can be seen that after the initial negative FiO_2 controller action from the AMPC, the AMPC closely resembles an overdamped response. A plot of the absolute estimation error during the simulation is given by Fig. 3-8, where it shows that it needs time to converge after the step input at 10 minutes. It had not converged prior as there was not a large enough amount of excitation in the system for estimation. The other spikes in the estimation error can be contributed to the quantization of the SpO_2.

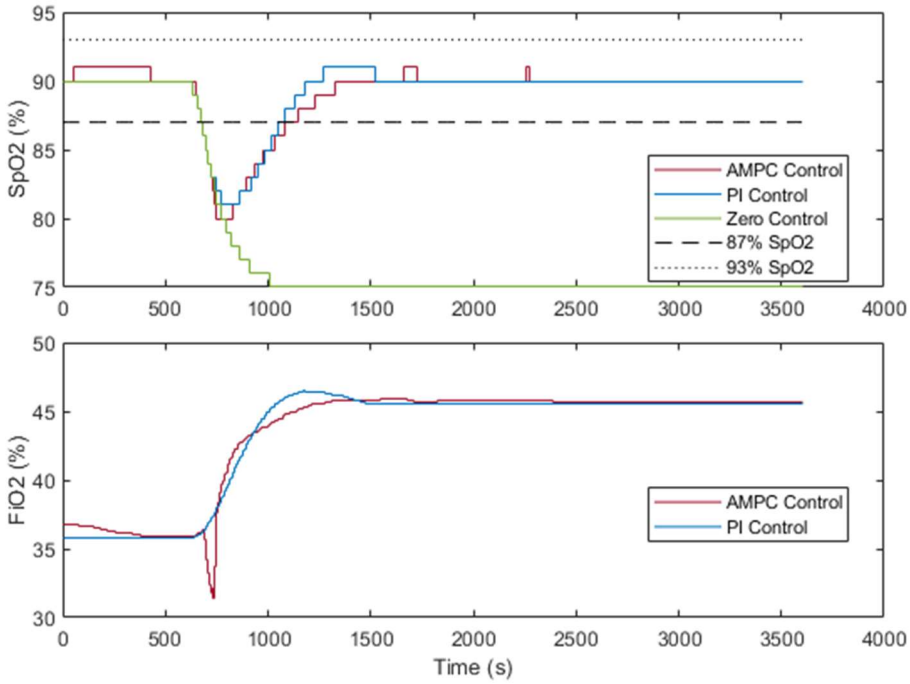

Fig. 3-7 Recovery from a Step HR and RR Disturbance

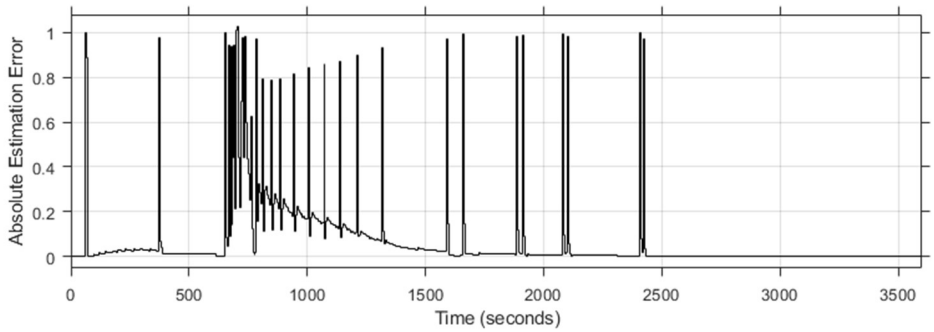

Fig. 3-8 Recovery from a Step HR and RR Disturbance absolute estimation error for the RPME.

The simulation was performed a second time, but with the colored noise disturbance added, and can be found in Fig. 3-9. From Fig. 3-9, it is seen that both controllers are able to adequately return to their reference setpoint even in the presence of this additional stochastic disturbance. Moreover, both controllers perform well in not amplifying the colored noise disturbance. Table 3-1 summaries the two simulations and the respective controller's ability to meet the design objectives of staying within the 87% to 93% SpO_2 ranges. First, it is seen that without the control, the model will not be able to recover from the desaturation alone, for either simulation. Additionally, both controllers could keep the SpO_2 within the bounds at least 26.5% of the time, even in the colored noise simulation. From these results, a general conclusion can be made where the AMPC, with no a priori knowledge of the model, could approach the performance of the tuned PI controller.

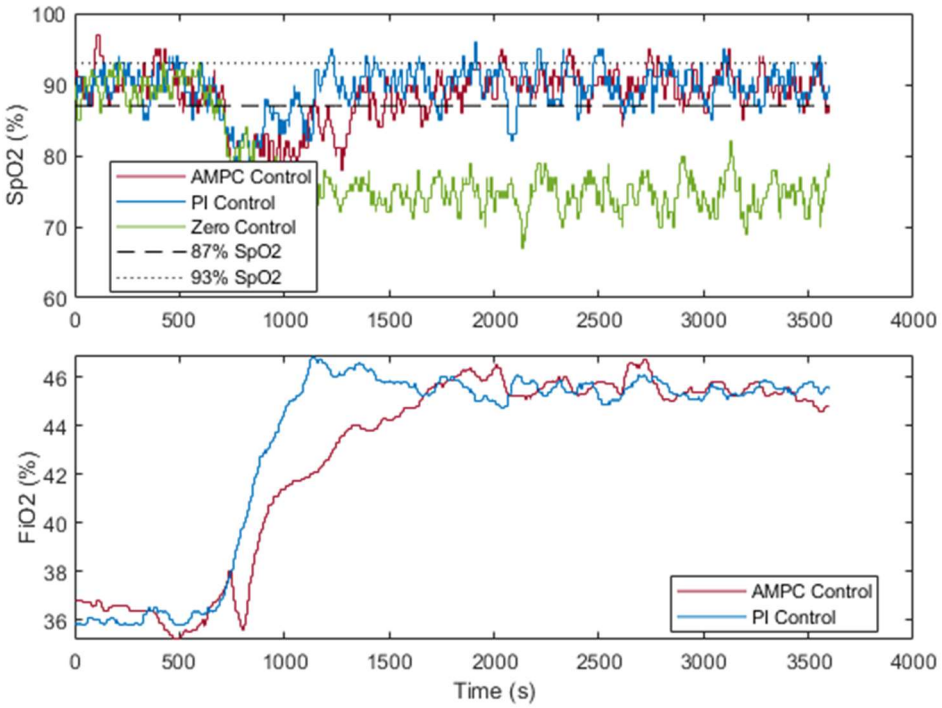

Fig. 3-9 Recovery from a Step HR and RR Disturbance, with colored noise

Table 3-1 Step input design objective results

Noise Model	Controller	Percent of Time Above 93%	Percent of Time Below 87%
OFF	AMPC	0	11.1
	PI	0	10.3
	Zero	0	81.1
ON	AMPC	5.3	21.2
	PI	4.6	14.8
	Zero	0.3	81.6

For the second set of simulations, a periodic RR disturbance, originally designed by [29] to test validation of the dynamic transfer function model described in [26] is utilized. This desaturation input begins with a box wave that is decreased from a magnitude of -2 to -12 every 800 seconds for a period of 160 seconds. From that, a sine

wave was superimposed that had a unitary amplitude and a frequency of 0.05 rad/s. This was then filtered through an 8th order Bessel filter. Some modifications were made to what was done in [29] for further stressing the controllers. The first modification was making this the disturbance signal for both the HR and the RR. Next, the entire signal was gained by three to increase the strength of the desaturations. With a maximum magnitude of 39, this was still within the allowable ranges. In addition, the wave was delayed by ten minutes. This was to not cause an immediate desaturation event at t = 0.

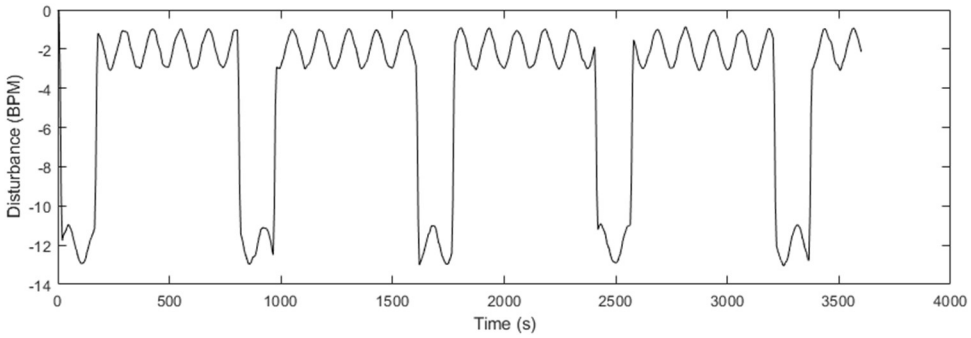

Fig. 3-10 RR disturbance input recreated from [29].

This periodic disturbance signal not only produced a strong periodic disturbance, but it could test the controller's ability to compensate from unexpected desaturation self-recoveries and the resulting hyperoxia. The deterministic simulations results are given in Fig. 3-11 and the simulation results with colored noise applied is given in Fig. 3-12. From Fig. 3-11, after the first periodic desaturation, the AMPC, is able to inject feedforward rejection of the HR and RR disturbances. This is confirmed when looking at the results for the design objectives given in Table 3-2, where the AMPC is able to stay within the SpO_2 design objectives 84.2% of the simulation with zero percent of the simulation above 93% SpO_2. This contrasts with the PI controller that is outside of the design objectives 42.6% of the simulation. It should be noted that there is still an initial negative FiO_2

response from the AMPC during the first periodic desaturation as the RPME converges. The superior performance of the AMPC carries over to the colored noise simulation as well where it continues to show successful feedforward disturbance rejection and better satisfaction of the design objectives than the PI controller. The AMPC stays within the design objectives 67.8% of the simulation compared to the PI controller at met the design objectives only 56.6% of the simulation.

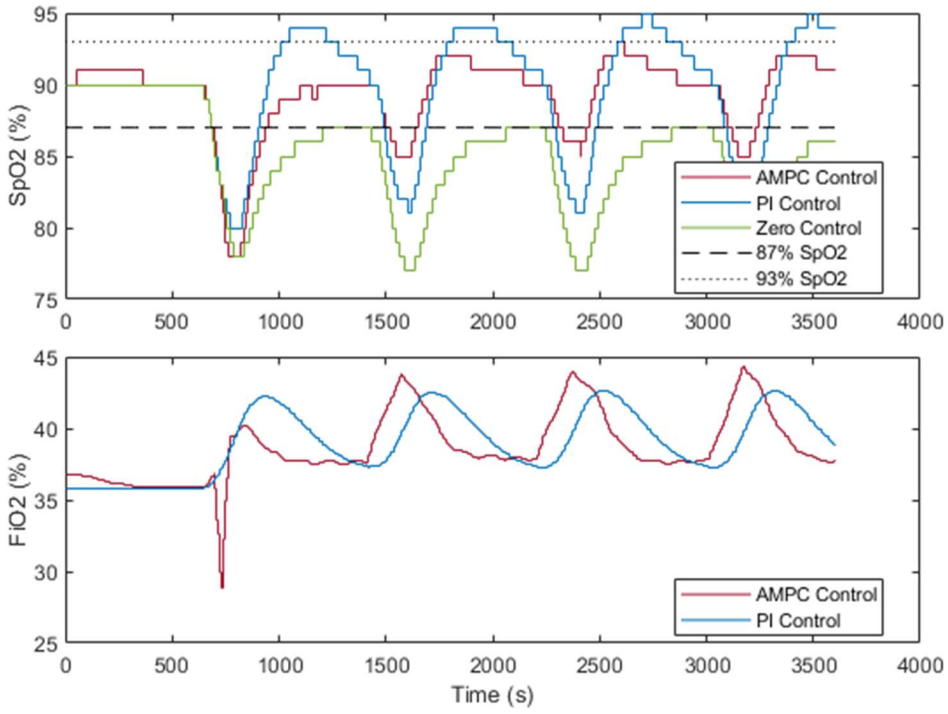

Fig. 3-11 Periodic Desaturation

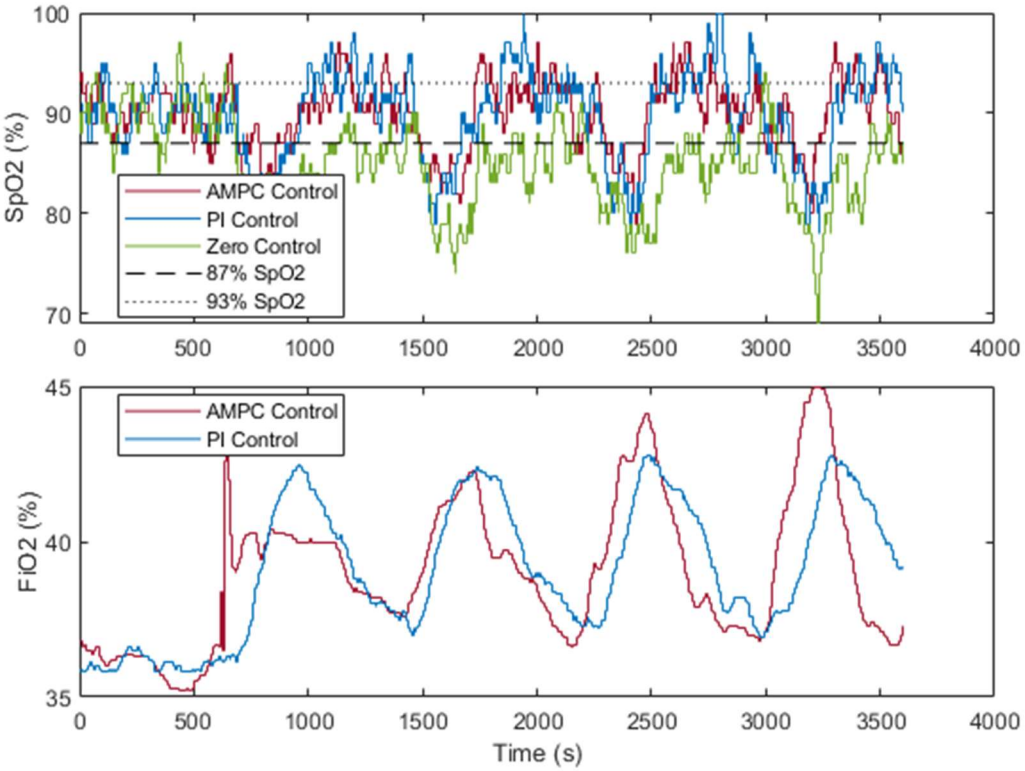

Fig. 3-12 Periodic Desaturation, with colored noise

Table 3-2 Periodic desaturation design objectives results

Noise Model	**Controller**	**Percent of Time Above 93%**	**Percent of Time Below 87%**
OFF	AMPC	0	15.8
	PI	21.4	21.2
	Zero	0	63.9
ON	AMPC	14.6	17.6
	PI	20.9	22.5
	Zero	1.4	63.2

4 Summaries, Conclusions, and Future Work

4.1 Polynomial System Identification Summary and Conclusions

The first major objective of this research was to investigate higher order modeling of the FiO_2, HR, and RR rate to SpO_2 and if a singular model could be carried forward for the purposes of simulation and controller design. An automated methodology for finding events for model estimation within clinical measurements was presented using an expanding window of data with a minimum of 80 samples on the forward derivative of the FiO_2 measurements over eleven days of clinical data measurements. These events were then down selected by ensuring a minimum SNR ratio of 4.5, leaving nineteen events from seven days of data containing a collection of positive and negative FiO_2 adjustments with corresponding HR and RR measurements. These nineteen events were then sorted into training data for model estimation, and validation data for model analysis.

With the training data, a parameter sweeps of all possible combinations of various sample delays, polynomial poles, and zeros for both the ARX and BJ polynomial model were created. This left a pool of 3,456 ARX models and 13,176 BJ models. With such a large collection of black-box models, a means to quantifiably narrow down the models for consideration was required. The metrics employed were picking a model based off having the smallest AIC, and the model having the smallest ΣMSE on both the training and validation data. Using those metrics, four models were selected for comparison. These four models were two from the ARX and two from the BJ; with two models per model structure representing the polynomial model order that minimized each respective metric. Comparisons involved analyzing the step responses for both their deterministic

and stochastic transfer functions as well as their performance in being able to simulate the clinical validation data.

From these comparisons, the overall winning model that was carried forward for controller design and simulation was the minimum AIC BJ model. This polynomial model was chosen because it was shown that picking BJ models could not only better represent and simulate the data better than the ARX models by having smaller mean of the ΣMSE, but their AIC, and thusly their ability to perform one step ahead prediction while using minimal model orders was similar to the lower complexity ARX models. Additionally, the AIC BJ model's colored noise model was more physically reasonable, as it had the smallest DC gain, 0.4%, compared to the other three models with 15.8% or more. This translates to more of the model being explained by the deterministic model than the stochastic noise model and therefore more captured dynamics.

Another important inference from the four winning models was that all the FiO_2 to SpO_2 dynamic relationships were modeled by a first order transfer function with delay. This lends to the body of research that a higher order model for these dynamics is not required. None the less, it was seen that higher order models for the HR and RR disturbances were needed.

4.2 Adaptive Model Predictive Control Conclusions

The other major objective of this research was being able to implement clinical best practices through an AMPC and successfully regulate the SpO_2 in the presence of both measured and unmeasured dynamics. A set of inequality constraints on the control and control rate of the FiO_2 was established from clinical best practices, such as 5% limits on

the adjustment of the FiO_2. Additionally, the quadratic cost function for the optimization of the AMPC controller action was tuned to focus on producing a conservative control rate. For the online estimation of the unknown model, a RPME was tuned to estimate the higher order dynamics of the minimum AIC BJ model, even in the presence of quantization.

For baselining the performance of the AMPC, a PI controller was tuned with a priori knowledge of the minimum AIC BJ model. Its design objective was to have a bandwidth frequency near the zero magnitude of the colored noise. By focusing on this design objective, the PI controller could balance performance while minimizing noise amplification.

Four simulations of different disturbances were conducted for evaluating the controller's ability to maintain SpO_2 target limits. The first disturbance simulation was subjecting the minimum AIC BJ model to just measured disturbances of step inputs to the HR and RR. The second simulation was the same step inputs to the HR and RR, but also using the colored noise of the minimum AIC BJ model. It was shown in Fig. 3-7 and Fig. 3-9 that the AMPC could approach the performance of the baseline PI controller. Quantification of this was given in Table 3-1 where the PI controller maintained its target limits for 80.6% simulation time compared to the 73.5% of the AMPC under extreme disturbances.

The third and fourth disturbance simulation focused on a periodic input to the HR and RR. This disturbance was used to evaluate the performance of the controllers against a frequent desaturation and possible unexplained self-recovery of the neonate. Furthermore, this disturbance input could be used to evaluate if the AMPC could

feedforward the reject the measured disturbances and perform better than the baseline PI controller once the RPME converged. The simulation results from both Fig. 3-11 and Fig. 3-12 showed that once the RPME converged, the AMPC could outperform the PI controller in the colored noise simulation by maintain the SpO_2 within the target ranges 67.8% of the simulation time compared to the PI controllers 56.6% result. All simulations were compared against zero control action.

Another conclusion is that quantization found in medical devices needs to be considered when designing controllers, as the sudden rounding can cause possible instabilities in the online model estimation. This was evidenced by the initial negative FiO_2 adjustments to the SpO_2 disturbance and absolute estimation errors of the RPME.

4.3 Future Work

There are three recommendations for future work from this research. The first would be looking at the possibility of obtaining better black box models from an even higher order HR and RR polynomials. By removing the need to estimate higher order FiO_2 models, the design space would be significantly reduced in size. It is suggested to use a genetic algorithm as it is a global optimization method that can handle integer constraints, such as selecting the polynomial model orders.

The largest limitation of the system identification process presented in this work was the reliance on needing to estimate the initial states for both the model regressions and model comparisons. A possible future research could be reusing the automated event finding algorithm to find SpO_2 desaturation events that still have FiO_2 adjustments. It is necessary to have FiO_2 adjustments in the extending window as otherwise the estimation

data would just a representation of the neonate's homeostasis, which can vary depending upon each neonate's maturity.

For the AMPC, it would be recommended to investigate the performance of the AMPC for different types of internal model structures than just the independent first order transfer functions from [29]. That means that an online higher order model could be recursively estimated for possible better feedforward disturbance rejection. Additionally, an investigation into methodologies to relate the quadratic programing weights to common design requirements such as closed loop bandwidth or frequency responses.

Appendix A: Winning Identified Models

A: Minimum AIC ARX Model at 5 second sample time

$$SpO_2(z) = z^{-4}\frac{0.07161\,z^{-1}}{1\,-\,0.9389\,z^{-1}}FiO_2 + \frac{0.02161z^{-1}}{1\,-\,0.9389\,z^{-1}}HR + z^{-2}\frac{0.01364\,z^{-1} - 0.008182z^{-2}}{1\,-\,0.9389\,z^{-1}}RR + \frac{1}{1\,-\,0.9389\,z^{-1}}e$$

A: Minimum ΣMSE ARX Model at 5 second sample time

$$SpO_2(z) = z^{-4}\frac{0.07511\,z^{-1}}{1\,-\,0.9369\,z^{-1}}FiO_2 + \frac{0.02291z^{-1}}{1\,-\,0.9369\,z^{-1}}HR + \frac{-0.004531\,z^{-1}\,+\,0.002896z^{-2}}{1\,-\,0.9369\,z^{-1}}RR + \frac{1}{1\,-\,0.9369\,z^{-1}}e$$

A: 1 Minimum AIC BJ Model at 5 second sample time

$$SpO_2(z) = z^{-1}\frac{0.06202\,z^{-1}}{1\,-\,0.9611\,z^{-1}}FiO_2 + z^{-8}\frac{-0.004934z^{-1}}{1\,-\,1.674\,z^{-1}\,+\,0.6851z^{-2}}HR + \frac{0.002798z^{-1}}{1\,-\,0.961z^{-1}}RR + \frac{1\,-\,0.991z^{-1}}{1\,-\,1.816\,z^{-1} + 0.8414\,z^{-2}}e$$

A: Minimum ΣMSE BJ Model at 5 second sample time

$$SpO_2(z) = z^{-4}\frac{0.04705\,z^{-1}}{1\,-\,0.9169\,z^{-1}}FiO_2 + \frac{0.00257z^{-1}}{1\,-\,1.832\,z^{-1} + 0.8527\,z^{-2}}HR + z^{-1}\frac{0.001237z^{-1}}{1\,-\,1.833\,z^{-1} + 0.8436\,z^{-2}}RR + \frac{1\,-0.6277z^{-1}}{1\,-\,1.399\,z^{-1} + 0.418\,z^{-2}}e$$

References

[1] V. Kumar, A. K. Abbas, and J. C. Aster, “Genetic and Pediatric Diseases,” in *Robbins Basic Pathology*, 10th ed., Philadelphia, PA: Elsevier, 2018, pp. 243–297.

[2] S. Fuentes and Y. S. Chowdhury, “Fraction of Inspired Oxygen,” in *StatPearls*, Treasure Island (FL): StatPearls Publishing, 2020.

[3] L. M. Willis, *Professional guide to diseases.*, Eleventh edition. Wolters Kluwer, 2020.

[4] H. Saneh, M. D. Mendez, and V. N. Srinivasan, “Cord Blood Gas,” in *StatPearls*, Treasure Island (FL): StatPearls Publishing, 2020.

[5] L. C. Chow, K. W. Wright, and A. Sola, “Can changes in clinical practice decrease the incidence of severe retinopathy of prematurity in very low birth weight infants?,” *Pediatrics*, vol. 111, no. 2, pp. 339–345, Feb. 2003, doi: 10.1542/peds.111.2.339.

[6] W. Baerts, P. M. A. Lemmers, and F. van Bel, “Cerebral Oxygenation and Oxygen Extraction in the Preterm Infant during Desaturation: Effects of Increasing FiO2,” *Neonatology*, vol. 99, no. 1, pp. 65–72, 2011, doi: 10.1159/000302717.

[7] W. Tin and S. Gupta, “Optimum oxygen therapy in preterm babies,” *Arch. Dis. Child. Fetal Neonatal Ed.*, vol. 92, no. 2, pp. F143–F147, Mar. 2007, doi: 10.1136/adc.2005.092726.

[8] The BOOST II United Kingdom, Australia, and New Zealand Collaborative Groups, “Oxygen Saturation and Outcomes in Preterm Infants,” *N. Engl. J. Med.*, vol. 368, no. 22, pp. 2094–2104, May 2013, doi: 10.1056/NEJMoa1302298.

[9] J. W. Salyer, “Neonatal and Pediatric Pulse Oximetry,” *Respir. CARE*, vol. 48, no. 4, p. 13, 2003.

[10] H. Bitterman, “Bench-to-bedside review: Oxygen as a drug,” *Crit. Care*, vol. 13, no. 1, p. 205, 2009, doi: 10.1186/cc7151.

[11] K. Lim *et al.*, “Oxygen Saturation Targeting in Preterm Infants Receiving Continuous Positive Airway Pressure,” *J. Pediatr.*, vol. 164, no. 4, pp. 730-736.e1, Apr. 2014, doi: 10.1016/j.jpeds.2013.11.072.

[12] B. Schmidt and R. K. Whyte, “Oxygen saturation target ranges and alarm settings in the NICU: What have we learnt from the neonatal oxygenation prospective meta-analysis (NeOProM)?,” *Semin. Fetal. Neonatal Med.*, vol. 25, no. 2, p. 101080, Apr. 2020, doi: 10.1016/j.siny.2020.101080.

[13] J. S. Gray, “The Multiple Factor Theory of the Control of Respiratory Ventilation,” *Science*, vol. 103, no. 2687, pp. 739–744, 1946.

[14] F. S. Grodins, J. Buell, and A. J. Bart, “Mathematical analysis and digital simulation of the respiratory control system.,” *J. Appl. Physiol.*, vol. 22, no. 2, pp. 260–276, Feb. 1967, doi: 10.1152/jappl.1967.22.2.260.

[15] Ph. Grevisse, H. Lecocq, and M. Demeester, “A Pulmonary Model for the Automatic Control of a Ventilator,” *IFAC Proc. Vol.*, vol. 8, no. 1, pp. 295–302, Aug. 1975, doi: 10.1016/S1474-6670(17)67566-9.

[16] C. Yu, W. G. He, J. M. So, R. Roy, H. Kaufman, and J. C. Newell, “Improvement in Arteral Oxygen Control Using Multiple-Model Adaptive Control Procedures,” *Biomed. Eng. IEEE Trans. On*, no. 8, pp. 567–574, 1987.

[17] O. S. Fathabadi *et al.*, "Assessment of validity and predictability of the FiO_2 – SpO_2 transfer-function in preterm infants," *Physiol. Meas.*, vol. 35, no. 7, pp. 1425–1437, Jul. 2014, doi: 10.1088/0967-3334/35/7/1425.

[18] O. Sadeghi Fathabadi *et al.*, "Characterisation of the Oxygenation Response to Inspired Oxygen Adjustments in Preterm Infants," *Neonatology*, vol. 109, no. 1, pp. 37–43, Nov. 2015, doi: 10.1159/000440642.

[19] I. R. Beddis, P. Collins, N. M. Levy, S. Godfrey, and M. Silverman, "New technique for servo-control of arterial oxygen tension in preterm infants.," *Arch. Dis. Child.*, vol. 54, no. 4, pp. 278–280, Apr. 1979, doi: 10.1136/adc.54.4.278.

[20] R. E. Dugdale, R. G. Cameron, and G. T. Tealman, "Closed-loop control of the partial pressure of arterial oxygen in neonates," *Clin. Phys. Physiol. Meas.*, vol. 9, no. 4, pp. 291–305, Nov. 1988, doi: 10.1088/0143-0815/9/4/001.

[21] A. Seyfang, S. Miksch, W. Horn, M. S. Urschitz, C. Popow, and C. F. Poets, "Using time-oriented data abstraction methods to optimize oxygen supply for neonates," in *Artificial Intelligence in Medicine*, vol. 2101, S. Quaglini, P. Barahona, and S. Andreassen, Eds. Berlin, Heidelberg: Springer Berlin Heidelberg, 2001, pp. 217–226.

[22] M. S. Urschitz *et al.*, "Automatic Control of the Inspired Oxygen Fraction in Preterm Infants: A Randomized Crossover Trial," *Am. J. Respir. Crit. Care Med.*, vol. 170, no. 10, pp. 1095–1100, Nov. 2004, doi: 10.1164/rccm.200407-929OC.

[23] E. P. Morozoff, J. Smyth, and others, "Evaluation of three automatic oxygen therapy control algorithms on ventilated low birth weight neonates," in *Engineering in Medicine and Biology Society, 2009. EMBC 2009. Annual International Conference of the IEEE*, 2009, pp. 3079–3082, Accessed: Sep. 05, 2015. [Online]. Available: http://ieeexplore.ieee.org/xpls/abs_all.jsp?arnumber=5332532.

[24] N. Claure *et al.*, "Multicenter Crossover Study of Automated Control of Inspired Oxygen in Ventilated Preterm Infants," *PEDIATRICS*, vol. 127, no. 1, pp. e76–e83, Jan. 2011, doi: 10.1542/peds.2010-0939.

[25] T. Keim, R. Amjad, and R. Fales, "Modeling and control of the oxygen saturation in neonatal infants," in *ASME 2009 Dynamic Systems and Control Conference*, 2009, pp. 105–112, Accessed: Sep. 22, 2015. [Online]. Available: http://proceedings.asmedigitalcollection.asme.org/proceeding.aspx?articleid=1648307.

[26] B. Krone, R. Fales, and R. Amjad, "Model of Neonatal Infant Blood Oxygen Saturation," in *ASME 2011 Dynamic Systems and Control Conference and Bath/ASME Symposium on Fluid Power and Motion Control, Volume 1*, Arlington, Virginia, USA, Jan. 2011, pp. 509–516, doi: 10.1115/DSCC2011-6182.

[27] T. Keim, R. Amjad, and R. Fales, "Modeling and Feedback Control of Inspired Oxygen for Premature Infants," in *ASME 2011 Dynamic Systems and Control Conference and Bath/ASME Symposium on Fluid Power and Motion Control*, 2011, pp. 501–508, Accessed: Sep. 22, 2015. [Online]. Available: http://proceedings.asmedigitalcollection.asme.org/proceeding.aspx?articleid=1638460.

[28] T. Keim, "Control of Arterial Oxygen Saturation in Premature Infants," Thesis, University of Missouri--Columbia, 2011.

[29] B. Krone, “Modeling and control of arterial oxygen saturation in premature infants,” Thesis, University of Missouri--Columbia, 2011.
[30] D. Quigley, “Control of arterial hemoglobin saturation in premature infants using H-infinity synthesis and performance specifications from best clinical practice,” M.S., University of Missouri--Columbia, 2013.
[31] A. A. A. Faqeeh, “Investigation of the performance of an automatic arterial oxygen controller,” Thesis, University of Missouri--Columbia, 2018.
[32] T. A. Shinn, Hou,Xuefeng, Faqeeh,Akram, R. Amjad, and R. Fales, “Estimation of First Order Model Parameters for Premature Infant SpO2 Responses,” 2018.
[33] J. W. Severinghaus, “Simple, accurate equations for human blood O2 dissociation computations.,” *J. Appl. Physiol.*, vol. 46, no. 3, pp. 599–602, Mar. 1979, doi: 10.1152/jappl.1979.46.3.599.
[34] M. U. Cavalcante, B. C. Torrico, O. da M. Almeida, A. P. de S. Braga, and F. L. M. da C. Filho, “Filtered model-based predictive control applied to the temperature and humidity control of a neonatal incubator,” in *2010 9th IEEE/IAS International Conference on Industry Applications - INDUSCON 2010*, Nov. 2010, pp. 1–6, doi: 10.1109/INDUSCON.2010.5739884.
[35] L. Ljung, *System identification : theory for the user*, 2nd ed. Prentice Hall, 1999.
[36] “Option set for bj - MATLAB bjOptions.” https://www.mathworks.com/help/ident/ref/bjoptions.html (accessed Nov. 11, 2020).
[37] “Akaike’s Information Criterion for estimated model - MATLAB aic.” https://www.mathworks.com/help/ident/ref/aic.html (accessed Nov. 09, 2020).
[38] K. J. Blinowska-Cieślak and J. Zygierewicz, *Practical biomedical signal analysis using MATLAB.* CRC Press, 2012.
[39] J. S. Milton and J. C. Arnold, *Introduction to probability and statistics : principles and applications for engineering and the computing sciences.*, 4th ed. McGraw-Hill, 2003.
[40] D. E. Seborg, *Process dynamics and control.*, 3rd ed. John Wiley & Sons, 2011.
[41] S. J. Qin and T. A. Badgwell, “A survey of industrial model predictive control technology,” *Control Eng. Pract.*, vol. 11, no. 7, pp. 733–764, Jul. 2003, doi: 10.1016/S0967-0661(02)00186-7.
[42] D. Simon, *Optimal state estimation : Kalman, H [infinity] and nonlinear approaches.* Wiley-Interscience, 2006.